UNIVERSITY OF CALIFORNIA
RIVERSIDE

$L1_0$-FePt Media for Next-Generation Data Storage Devices

A Dissertation submitted in partial satisfaction
of the requirements for the degree of

Doctor of Philosophy

in

Electrical Engineering

by

Robert Anthony Fernandez

August 2010

Dissertation Committee:

Dr. Sakhrat Khizroev, Chairperson
Dr. Ilya Dumer
Dr. Alexander A. Balandin

The Dissertation of Robert Anthony Fernandez is approved:

_____

_____

_____

Committee Chairperson

University of California, Riverside

ACKNOWLEDGEMENTS

I would like thank my advisor, Dr. Sakhrat Khizroev, as well as my labmates, Chen Zhang, Beomseop Lee, Engin Akin, and Nissim Amos, for their help on this work.

DEDICATION

I would like to dedicate this dissertation to all my friends and family who have supported me during my graduate studies, and especially my brothers Ralph and Ryan, my sister Sarah, my father Ralph, and my mother Ida.

ABSTRACT OF THE DISSERTATION

$L1_0$-FePt Media for Next-Generation Storage Devices

by

Robert Anthony Fernandez

Doctor of Philosophy, Graduate Program in Electrical Engineering
University of California, Riverside, August 2010
Dr. Sakhrat Khizroev, Chairperson

$L1_0$-ordered FePt thin films are a leading candidate for next-generation magnetic recording, such as bit-patterned media (BPM), heat-assisted magnetic recording (HAMR), and multilevel three-dimensional (ML3D) magnetic recording, because of their excellent material properties. Its high magnetocrystalline anisotropy of ~ 10^8 ergs/cm^3 allows for grain sizes less than a few nanometers while maintaining good thermal stability. It also has been demonstrated that $L1_0$-FePt can achieve coercivity greater than 10 Tesla. However, achieving the $L1_0$-phase requires post-annealing and/or deposition at elevated substrate temperature. In this work, the magnetic and microstructural properties of FePt thin films were investigated and improved for the use in perpendicular magnetic recording. FePt thin films were then fabricated on pre-patterned substrates for the use in BPM, with a heat sink layer for the use in HAMR, and with two magnetic layers for the use in ML3D magnetic recording.

Table of Contents

List of Figures

I. Introduction

The hard disk drive (HDD) industry has been around for over sixty years. Like most industries, it has seen its ups and downs but has continually prospered as the technology advanced. In the early 2000s, the HDD industry underwent a subtle, but drastic change as it went from longitudinal magnetic recording to perpendicular magnetic recording. This change allowed the HDD industry to maintain its rapid growth in areal density, making more and more storage on smaller and smaller area. However, soon the HDD industry must make another change if it hopes to survive. This change involves finding new magnetic materials and new storage technologies. This dissertation involves research to solve both those problems. FePt is widely regarded as a candidate material to replace conventional materials. In this dissertation, an introduction to magnetism and the hard disk drive industry is given. Next, research on fabricating and characterizing FePt thin films as a next-generation HDD material is shown. Lastly, FePt media is then incorporated into future HDD technologies, which are bit-patterned media, heat-assisted magnetic recording media, and 3-D magnetic recording media.

II. Introduction to Magnetism

The term magnetism is used to describe how a material responds on the microscopic level to an applied magnetic field. Magnetism, at its root, arises from two sources. One source of magnetism is due to electric currents, or more specifically, moving electric charges which create magnetic fields. One example is an electromagnet, where electric current moves through wire coils to create a magnetic field. The second

source of magnetism comes from a particle's nonzero "intrinsic" magnetic moments. Just as each particle, by its nature, has a certain mass and charge, each particle has a certain magnetic moment. For most materials, the net magnetic moment is zero, and thus only exhibits magnetic behavior when a magnetic field is applied, such as a paramagnet or diamagnet. However, some materials maintain an overall non-zero magnetic moment and exhibit magnetic behavior with or without an applied magnetic field, such as a ferromagnet. The magnetic state of a material depends on temperature and sometimes other variables such as pressure and applied magnetic field, so that a material may exhibit more than one form of magnetism depending on these variables.

A. Diamagnetism

Diamagnetism is the property of an object which causes it to create a magnetic field in opposition to an externally applied magnetic field, thus causing a repulsive effect. More specifically, an external magnetic field alters the orbital velocity of electrons around their nuclei, thus changing the magnetic dipole moment in the direction opposing the external field. Diamagnetism is a very general phenomenon because all paired electrons, including the electrons of an atom, will always make a weak contribution to the material's response. However, for materials that show some other form of magnetism, the diamagnetic effect is completely overpowered. Substances that only display diamagnetic behavior are diamagnetic materials, or diagmagnets. Materials that are said to be diamagnetic are those that are usually considered by non-physicists to be "non-magnetic",

and include water, carbon and most other organic compounds, and many metals such as copper, particularly those with many core electrons, such as mercury, gold and lead.

B. Paramagnetism

Paramagnetism is a form of magnetism that occurs only in the presence of an externally applied magnetic field. Paramagnetic materials are attracted to magnetic fields and hence have a positive magnetic susceptibility. The magnetic moment induced by the applied field is linear to the field strength applied and rather weak. It typically requires a very sensitive analytical balance to detect the effect. Unlike ferromagnets, paramagnets do not retain any magnetization in the absence of an externally applied magnetic field because thermal motion causes the spins to become randomly oriented without it. Thus the total magnetization will drop to zero when the applied field is removed. This is often why paramagnetic materials are measured at extremely low temperatures. Even in the presence of a magnetic field there is only a small induced magnetization because only a small fraction of the spins will be oriented by the field. This fraction is proportional to the field strength and this explains the linear dependency. Some examples of paramagnetic materials are tungsten, aluminum, and magnesium.

C. Ferromagnetism

Ferromagnetism is the basic mechanism by which certain materials form permanent magnets, or are attracted to magnets. In physics, several different types of magnetism are distinguished, with ferromagnetism being the strongest type. It is the only type that can produce forces strong enough to be felt, and is the type of magnetism

responsible for the common phenomena of magnetism encountered in everyday life, such as refrigerator magnets. All permanent magnets, that is, materials that can be magnetized by an external magnetic field and *remain* magnetized after the external field is removed, are either ferromagnetic or ferromagnetic, as are other materials that are noticeably attracted to them.

Historically, the term ferromagnet was used for any material that could exhibit spontaneous magnetization, a net magnetic moment in the absence of an external magnetic field. While this general definition is still commonly used, more accurately, there are different classes of spontaneous magnetization when there is more than one magnetic ion per primitive cell of the material. Therefore, a material is ferromagnetic only if all of its magnetic ions add a positive contribution to the net magnetization. If some of the magnetic ions "subtract" from the net magnetization, that is, are partially anti-aligned, then the material is ferrimagnetic. If the magnetic moments of the aligned and anti-aligned ions cancel each other out completely so that there zero net magnetization, then the material is antiferromagnetic. All of these alignment effects only occur at temperatures below a certain critical temperature, called the Curie temperature for ferromagnets and ferrimagnets, or the Néel temperature for antiferromagnets. The most common ferromagnetic materials are iron, cobalt, nickel and gadolinium.

Ferromagnetism is a property not just of the elemental makeup of a material, but of its crystalline structure and microscopic organization. For example, there are ferromagnetic metal alloys whose constituents are not themselves ferromagnetic. These materials are called Heusler alloys, named after Fritz Heusler. Also, there are

nonmagnetic alloys which are composed of mostly ferromagnetic metals, such as stainless steel, which is mostly iron. Amorphous (non-crystalline) materials can also be ferromagnetic. This is usually done by rapid quenching (cooling) of a liquid alloy. For ferromagnetic thin films, the crystal structure is controlled by the use of certain seed layers or substrates, and/or the deposition conditions, such as pressure, temperature and power. Recently, a relatively new class of exceptionally strong ferromagnetic materials has become more common. These rare-earth magnets contain lanthanide elements that are known for their ability to carry large magnetic moments in well-localized f-orbitals. These rare-earth magnets are used in magnetic measurements systems with well above 3 Tesla and as high as 16 Tesla, and require liquid helium and liquid nitrogen systems to keep the magnets from overheating.

D. Anitferromagnetism

In materials that exhibit antiferromagnetism, the magnetic moments of atoms or molecules, usually related to the spins of electrons, align in a regular pattern with neighboring spins pointing in opposite directions. This is, like ferromagnetism and ferrimagnetism, a manifestation of ordered magnetism. Generally, antiferromagnetic order only exists at sufficiently low temperatures, vanishing at and above a certain temperature, known as the Néel temperature, named after Louis Néel, who had first identified this type of magnetic ordering. Above the Néel temperature, the material is typically paramagnetic. When no external field is applied, the antiferromagnetic structure corresponds to a vanishing total magnetization. In a field, a kind of ferrimagnetic behavior may be displayed in the antiferromagnetic phase, with the absolute value of one

of the sublattice magnetizations differing from that of the other sublattice, resulting in a nonzero net magnetization.

Various microscopic interactions between the magnetic moments or spins may lead to antiferromagnetic structures. In the simplest case, one may consider an Ising model on a simple cubic lattice, with couplings between spins at nearest neighbor sites. Depending on the sign of that interaction, ferromagnetic or antiferromagnetic order will result. Geometrical frustration or competing ferromagnetic and antiferromagnetic interactions may lead to different and/or more complicated magnetic structures.

Antiferromagnetism plays a crucial role in giant magnetoresistance, as had been discovered in 1988 by the Nobel Prize winners Albert Fert and Peter Grünberg, awarded in 2007. Antiferromagnets can couple to ferromagnets, for instance, through a mechanism known as exchange bias, in which the ferromagnetic film is either grown upon the antiferromagnet or annealed in an aligning magnetic field, causing the surface atoms of the ferromagnet to align with the surface atoms of the antiferromagnet. This provides the ability to "pin" the orientation of a ferromagnetic film, which provides one of the main uses in spin valves, which are the basis of magnetic sensors including modern hard drive read heads and magnetic tunnel junctions. The temperature at or above which an antiferromagnetic layer loses its ability to "pin" the magnetization direction of an adjacent ferromagnetic layer is called the blocking temperature of that layer and is usually lower than the Néel temperature. Some examples of antiferromagnetic materials are metals such as chromium, alloys such as iron manganese, and oxides such as nickel oxide.

E. Ferrimagnetism

A ferrimagnetic material is one in which the magnetic moments of the atoms on different sublattices are opposed, as in antiferromagnetism, however, in ferrimagnetic materials, the opposing moments are unequal and do not cancel each other out completely. Thus, a net nonzero magnetization remains. This happens when the sublattices consist of different materials or ions. Ferrimagnetic materials have high resistivity and have anisotropic properties. The anisotropy is actually induced by an external field. When this applied field aligns with the magnetic dipoles it causes a net magnetic dipole moment and causes the magnetic dipoles to precess at a frequency controlled by the applied field, called Larmor or precession frequency.

Ferrimagnetic materials are like ferromagnets in that they hold a spontaneous magnetization below the Curie temperature, and show no magnetic order above this temperature. However, there is sometimes a temperature below the Curie temperature at which the two sublattices have equal moments, resulting in a net magnetic moment of zero. This is called the magnetization compensation point. This compensation point is readily observed in garnets and rare earth-transition metal alloys. Furthermore, ferrimagnets may also exhibit an angular momentum compensation point at which the angular momentum of the magnetic sublattices is compensated. This compensation point is a crucial point for achieving high speed magnetization reversal in magnetic memory devices. Ferrimagnetic materials are also used to produce optical isolators and circulators. Ferrimagnetism is exhibited by ferrites and magnetic garnets. The oldest-known magnetic substance, magnetitie (iron(II,III) oxide) is ferrimagnetic, though originally believed to

be ferromagnetic before the discovery of ferrimagnetism and antiferromagnetism. Other ferrimagnetic substances include yttrium iron garnet and ferrites composed of iron oxides and other elements such as aluminum, cobalt, nickel, manganese and zinc.

III. Introduction to Hard Disks Drives

Hard disk drives (HDDs) have traditionally been used in computers since the late 1950s when IBM introduced random access method of accounting and control (RAMAC).[1] The first-generation hard disk drives were expensive and extremely bulky but pioneered the random access feature for the main frame computers of that era. Hard disk drives improved over time and were incorporated into personal computers in the 1980s. Today, HDDs can be found everywhere in consumer electronics applications. Digital cameras, iPods, cell phones, video game consoles, and many other devices use HDDs to store information. Figure 1 shows an image of IBM's RAMAC, composed of fifty 24-inch disks with a 4.4 MB capacity and Western Digital's external hard drive, composed of two 2.5-inch disks with a capacity of 1 TB, illustrating how HDDs have gotten smaller with larger storage capacities over time. In this decade, about 500 billion HDDs are produced every year in order to satisfy the needs of computer and consumer electronics (CE) applications. Such a high demand is a large driving factor in HDD research in order to maintain its competitive edge over other technologies such as flash memory or optical storage devices. The HDD industry is constantly looking for ways to reduce cost, reduce size, and increase the areal density of HDDs.

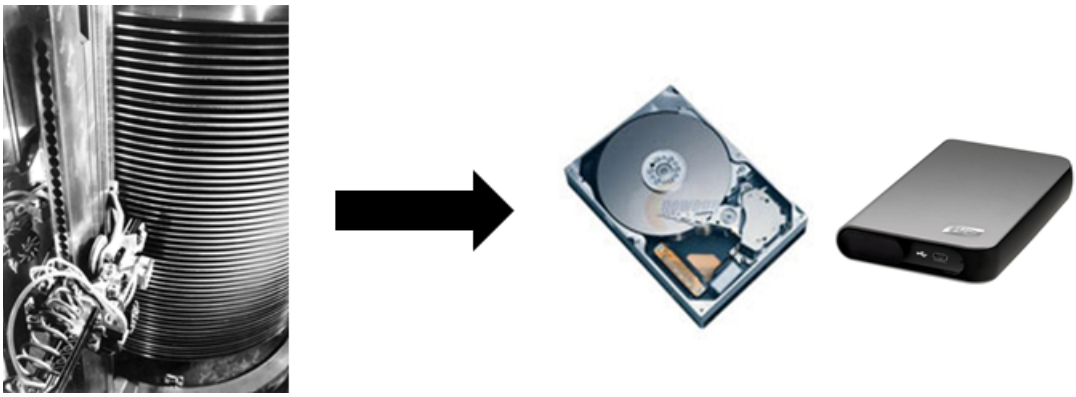

Fig. 1. On the left, an image of IBM's RAMAC in 1956, composed of fifty 24-inch disks with a storage capacity of 4.4 Megabytes. On the right, an image of Western Digital's external hard drive in 2009, composed of two 2.5-inch disks with a 1 Terabyte capacity.

Until recently, hard disk drives employed longitudinal magnetic recording (LMR) technology to store information. In longitudinal recording, magnetizations that lie longitudinally (parallel to the disk surface) are used for storing information. Alternative technologies such as perpendicular magnetic recording (PMR), in which magnetizations lie perpendicular to the disk surface, were proposed in the late 1970s to overcome some potential problems with longitudinal magnetic recording.[2-4] However, LMR was able to stay competitive for all these years and delayed its rival technology. Only recently has PMR technology replaced LMR technology in current HDDs. This was due to the risks, problems, and huge investment needed in making perpendicular magnetic recording. In fact, this huge investment is what delayed PMR for decades, until the HDD industry was forced use PMR to due to the limitations of LMR. Some of these limitations, such as the superparamagnetic limit and signal-to-noise ratio will be discussed later. The introduction of magnetically soft underlayers (SULs) and improvements in read and write head design and materials have also paved the way for PMR to replace LMR.

A. Overview of Longitudinal Magnetic Recording

The first magnetic recording device was demonstrated and patented by the Danish inventor Valdemar Poulsen in 1898, when Poulsen made a magnetic recording of his voice on a length of piano wire.[1] Magnetic recording relies on two basic principles: (i) Magnets produce strong magnetic fields at the poles. This field can be used for reading information. (ii) The polarity of the magnets itself can be changed by applying external fields. This provides a possibility of writing information. Therefore, a magnetic recording device would need to have the following key components: a recording medium to store information, a writer head to produce localized magnetic fields for writing information, and a read sensor to convert the magnetic field from the media to electrical (voltage) signals for reading information. There are many other components to position the head, to interpret the voltages into bits, and so on.

In the first few generations of hard disk drives, and in many tape storage devices, such as VCRs, a particulate medium (which is essentially a mixture of magnetic particles in a binder) was used.[1] The magnetic media used was primarily iron(III) oxide; however, this particulate medium cannot have a high saturation magnetization because the saturation magnetization of the magnetic material will be diluted by the binder. In the earlier days, a high saturation (or remanent) magnetization was required from the recording media, as the signal produced will be proportional to the product of the remanent moment and thickness of the media and the heads were not sensitive enough to detect a weak signal. Another problem was that the coercivity of the particulate media could not be easily tailored to meet the high-density requirements. Therefore, thin film

media was considered as an alternative for HDDs because of it can provide high saturation/remanent magnetization and higher coercivity. Also, thin film media provided smooth surfaces, allowing for easier reading and writing. Particulate media was phased out in the 1980s which brought about longitudinal magnetic recording. In this section, some of the requirements of longitudinal recording media and the ways they were achieved are described.

1. Granular media

Thin film media are usually deposited by dc and rf magnetron sputtering onto glass or aluminum substrate disks. Current recording media have several layers that serve different purposes in order to achieve desired performance. However, it is the magnetic layer where information is actually stored. The magnetic layer produced by sputtering is a polycrystalline material. Therefore, the grains of the recording medium would have random orientations with respect to the film plane and with respect to the track direction as well. Furthermore, they would also be arranged in random positions and sizes. Because of this randomness of the grains used in storing the information, a group of grains are used to store information. A group of grains can range from as few as 20 grains to several hundred, depending on the quality of the media, the read/write head and the overall technology of the hard disk drive. Older generations of HDDs will use more grains per bit than new generations. This group of grains acts as a larger, single magnet, called a "bit," which is then used to store information by aligning the net magnetization of all the grains in one direction. These bits are then used to store the "1's" and "0's" of binary code. The borders of these bits make up the "bit boundary," which is one of several factors that

determine the signal-to-noise ratio (SNR). Figure 2 is a TEM image of granular magnetic media. The inset illustrates the randomness of easy-axis orientation and randomness of the size of grains. The bit boundary in Figure 2 is designated by a. The signal-to-noise ratio is approximated by the expression

$$SNR = 10 \log(N), \quad (1)$$

where N is the number of grains in a bit. To some extent, the SNR at a particular linear density is an indicator of how reliably the bits could be read out at that linear density. Therefore, SNR is a key indicator of the quality of the recording performance of a recording medium. Equation (1) indicates that increasing the number of grains would help increase the SNR. Therefore, one way to increase the SNR of the recording medium is to reduce the grain size and grain size distribution, which would increase the number of grains in the bit area. Simply incorporating more grains per bit without reducing the grain size would also increase the SNR, but at the same time reduce the areal density of the recording medium. Grain size reduction can be achieved by the use of seed layers and/or underlayers with small grains sizes or from the magnetic layer itself, which usually entails doping the magnetic layer with another material to further isolate the magnetic grains.[5-15]

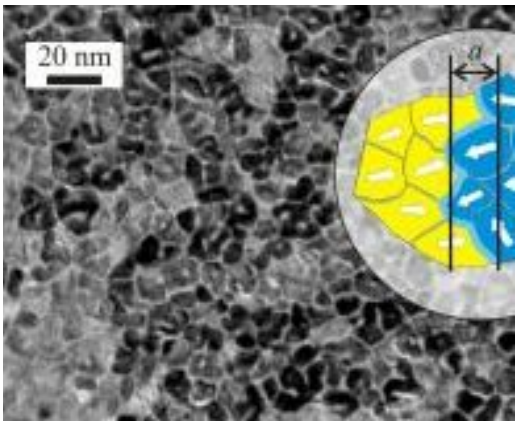

Fig. 2. A TEM image of granular media. The inset shows the randomness of easy-axis oreintations and the bit boundary, with length a.

2. Orientation of the grains

Another requirement for improving magnetic recording media is to have well-oriented grains. In the case of longitudinal media, the grains should be oriented parallel to disk and also parallel to the track direction. When the thin film media is sputter-deposited, the randomness of grain size and magnetization orientation occurs in order to minimize the energy of the film. However, one way to minimize the randomness of orientation is to improve the number of grains that have an easy axis along the film plane. This can be achieved by using various underlayers such as Cr, CrV, CrTi, CrMo, or combinations of these by improving the *c*-axis orientation of the magnetic layer parallel to the film plane.[5,6,11,16-20] It has also been reported that the use of intermediate layers help to improve the easy axis orientation by improving the lattice matching between the Cr underlayers and the CoCrPt-based magnetic layers.[21] In addition to using an underlayer and an intermediate layer to improve the in-plane easy axis orientation, another way to minimize the randomness is to increase the number of grains that have an easy axis orientation parallel to the track direction. Figure 3 illustrates the magnetization

orientation for different media configurations. A recording medium in which the magnetic moments are randomly oriented with respect to the plane and with respect to the track [Figure 3(a)] would have the lowest SNR. This is because, in such a recording medium, the component of magnetization that lies parallel to the disk surface or track direction is low. This will lead to a reduction in the signal and an increase in the noise. The SNR can be increased by maximizing the number of grains that are oriented parallel to the disk surface [Figure 3(b)]. These can be achieved by using Cr-based underlayers as previously discussed. By orienting the magnetization of the grains along the track direction as well as parallel to the disk surface, further increase of SNR can be obtained [Figure 3(c)]. This can be achieved by a texturing process, which can lead to an increased orientation ratio. Figure 3(d) shows the ideal configuration of orienting magnetic grains for longitudinal media for obtaining very high SNRs. However, such a configuration is not possible to achieve experimentally.

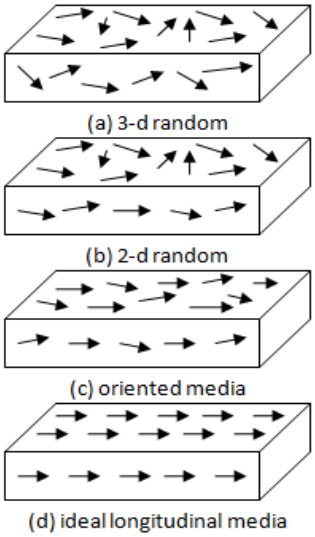

Fig. 3. The randomness of easy axis orientation: (a) three-dimensional random, (b) two-dimensional random, (c) oriented media, and (d) ideal orientation.

3. Challenges of longitudinal magnetic recording

One of the challenges of LMR that was highly researched was reducing the exchange coupling between the grains. Even if the magnetic grains are very small, having high exchange coupling enlarges the magnetic domains of the media, which in turn increases the smallest possible bit size, which then reduces the areal density of the film. Some initial work to reduce exchange coupling relied on the surface morphology of the underlayers. A rough surface was obtained by depositing very thick underlayers, which led to a physical separation between magnetic layer grains.[22] When the grains were separated from each other, exchange coupling between the grains of the recording layer was reduced. However, having thick underlayers also led to a larger grain size in the recording layer due to the large roughness. Therefore, better methods were needed to separate the magnetic layer grains from each other. One such method to obtain exchange decoupling was by compositional segregation at high temperatures.[11] Also, it is possible to sputter a recording medium that has two regions with different properties. The core of the grain would have magnetic properties and the grain boundary would have nonmagnetic properties. Therefore, the nonmagnetic grain boundary would serve as a shield from one grain to another, reducing the exchange coupling. Elements such as Ta, Cr, and B have been added to the magnetic layer to reduce the exchange coupling and also improve the grain isolation which produced much smaller grain sizes.[23,24]

In magnetic recording, the energy barrier that prevents the magnetization of a particle from flipping is proportional to the anisotropy energy K_uV, where K_u is the anisotropy constant of the material and V is the volume of the grain. It is this anisotropy

energy that helps to store the bit and make hard disk drives a nonvolatile storage device. If the particle is to switch its magnetization from one direction to another, energy has to be supplied to overcome the energy barrier. An applied external field, which alters the energy barrier, is usually required to switch the direction of magnetization. In the case of magnetic recording, the external field is applied using the write head, which in actually is just an electromagnetic with nanometer scale dimensions. In the previous section, it was discussed that exchange decoupling and small grain size are imperative for having high density LMR media. However, since K_u is an intrinsic property of the material, and thus, fixed, decreasing the grain size (V) reduces the energy barrier for magnetization reversal. When the anisotropy energy K_uV gets lower, the thermal energy, k_BT, starts to overcome the anisotropy energy and makes the magnetization thermally excited and reversed. This phenomenon, where the magnetic particles could reverse their magnetization without any external field, is called superparamagnetism. Since a recording medium is composed of grains with different sizes, some of the smaller grains would be more susceptible to thermal switching. It has been reported that the data will be lost even if 5% of the magnetization reverses due to thermal excitations.[25,26] This thermal stability factor, K_uV/k_BT, is referred to as the superparamagnetic limit, because there is a limit to how small the grains the recording media can while without becoming thermally unstable. The HDD industry were no longer able to increase the areal density of HDDs by simply scaling down, new methods and technologies were needed.

The superparamagnetic limit of longitudinal recording technology is the physical limit that paved the way for perpendicular magnetic recording technology. However, the

bottleneck for LMR is still based on the available write head materials to write information. It is possible to make longitudinal recording media that can provide thermal stability at higher areal densities than the present densities, however, writing and reading information from such media remains a challenge. The transition from longitudinal magnetic recording to perpendicular magnetic recording brought about improvements not only in the media, but also in how to write and read information.

B. Overview of Perpendicular Magnetic Recording

Demagnetizing fields are experienced in any ferromagnetic or ferrimagnetic system and are expressed as

$$H_d = -NM, \tag{2}$$

where N is the demagnetization tensor and M is the magnetization vector. N depends on the shape and direction of the magnet. The rule of thumb is that the demagnetization field is stronger when the magnetic charges or the magnetic poles are nearer. In longitudinal recording, as the linear density increases, the distance between the magnetic charges or the magnetic poles decreases, as shown in Figures 4(a)-4(c). This leads to an increased demagnetizing field.

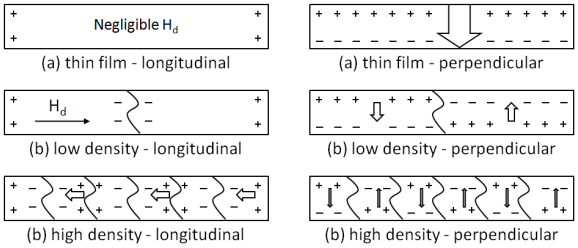

Fig. 4. Illustration of magnetic charges and the associated demagnetizing fields of longitudinal and perpendicular recording for (a) thin film, (b) low density, and (c) high density. The arrows indicate the direction of demagnetizing field. Block arrows are used to show the higher strength of demagnetizing field.

However, in perpendicular recording, as the linear density increases, the demagnetizing field decreases. The reason lies in the orientation of the magnetic tracks. Consider these tracks to be tiny magnets with a north pole and south pole at each end (designated by + and – signs in Figure 4). These poles are where the strongest fields are located. In LMR, these tracks lie horizontally, thus, the edges of the tracks (poles) are lined up against each other and experience the strongest forces possible from its neighboring tracks. In perpendicular recording, these tracks are lined up perpendicularly side-by-side. Thus, the area where the tracks come into contact with one another experience a much weaker force coming from the magnetic field of neighboring tracks.

Although several configurations for perpendicular recording have been proposed, the invention of double-layered perpendicular recording media and the single-pole head design proved crucial for the superiority of perpendicular recording over longitudinal recording. Together, these inventions provide a superior writing performance in perpendicular recording than is possible in longitudinal recording. Figure 5 illustrates the writing process in longitudinal and perpendicular recording. In longitudinal recording, if the fringing field from the head is higher than the coercivity of the grain, the magnetization will be reversed and writing will be achieved. In the recording medium, the grains have different energy barriers because of the distribution in size and anisotropy constant. Therefore, in order to reverse all the grains at smaller time scales for hard disk recording, the field from the head is made to be two to three times the coercivity of the material. Depending on the distance of the head from the track, the fringing field (H_f) varies, but is approximately $2\pi M_s$, where M_s is the saturation magnetization of the

material. However, the field in the gap (H_g) of the ring head is known to be $4\pi M_s$. Thus, in longitudinal recording, the weaker field is used to write information. In perpendicular recording technology, H_g is used for writing information. This is achieved through the use of a magnetically soft underlayer (SUL) and a single-pole head, as illustrated in Figure 5(b). Since the SUL is highly permeable, it acts as a magnetic mirror, which brings the magnetic flux of the pole head through the recording layer and into the SUL. It can be visualized that in perpendicular recording the media is virtually placed in the gaps of the poles and hence under higher writing fields. The use of this higher writing field is useful for two reasons: (1) faster writing times can be achieved and (2) higher anisotropy media can be used. Faster writing times are necessary to stay competitive over other recording technologies such as flash and optical storage. By using higher anistropy media, smaller grains and bits can be used to store information while still remaining thermally stable. Thus, higher areal densities can be achieved in perpendicular recording than in longitudinal recording.

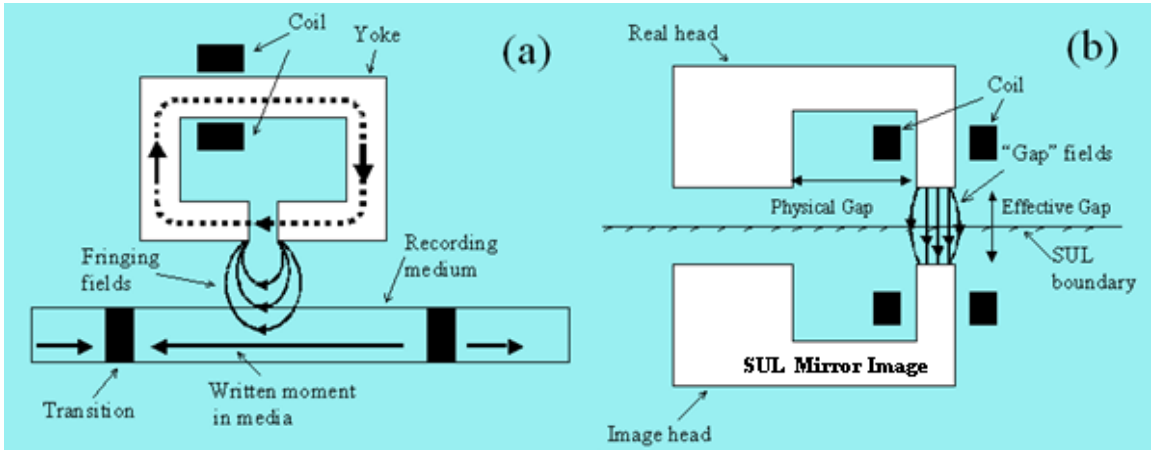

Fig. 5. Writing process in (a) longitudinal and (b) perpendicular recording. In perpendicular recording technology, the medium is virtually placed in the pole gaps between the head and the mirror image in the SUL.

In spite of several advantages that perpendicular recording technology had over longitudinal recording technology, PMR was not given serious thought until early this century. Early areal density demonstrations on perpendicular recording media were lagging behind that of longitudinal recording. One reason was longitudinal media were able to achieve a smaller grain size than perpendicular media. Also, PMR media studied in the early 2000s had higher compositions of Cr in order to obtain the desired grain boundary segregation. However, the presence of more Cr also led to a reduction in the anisotropy constant of the grains. With a reduced anisotropy constant, some grains are more susceptible to thermally assisted switching. Such grains will be a source of dc noise. In addition, the SUL issues were also not solved, which led to an inferior performance of perpendicular recording. Despite these setbacks, perpendicular recording became the focal point of the HDD industry when an areal density limit of 130 Gbits/in.^{2} was reached in longitudinal recording. For the past five years or so, significant improvements were made in the perpendicular recording. The improvements came from the recording layer and soft underlayers of the recording media, and also the writing heads, which made perpendicular recording technology more promising.[27-32]

1. Description of various layers and their functions

Figure 6 shows various functional layers, such as the soft underlayer, recording layer, etc., of a typical double-layered perpendicular recording medium. In more practical designs, there may be more than one layer involved for every function. The most advanced or exploratory designs may have a totally different structure than described. However, for the sake of simplicity, only a simple design is shown to illustrate the

function of each layer. The recording medium is normally deposited on an AlMg alloy disk precoated with a NiP layer or a glass substrate disk of a dimension suitable for its particular application. For example, server, desktop and large external HDDs typically use disk substrates with diameters of 3.5 in. or more. The substrate disk diameter for laptops and smaller, portable hard disk drives are 2.5 in. For small electronic devices such as MP3 players, etc., HDDs with a diameter range of 1-2 inches are used. Most of the layers in a hard disk medium are deposited by the sputtering process. Prior to the deposition of any layer, the substrates are cleaned to remove chemical and particle contaminants. Then, the substrate is first coated with an adhesion layer or interface layer, such as Ta, Ti or an alloy of these materials. This layer helps in improving the adhesion of the SUL and all other layers with the substrate. The next layer deposited is the soft magnetic underlayer. The SUL helps in conducting flux from the writing pole of the head to the trailing pole, as previously mentioned. On top of the SUL, some intermediate layers are deposited with or without seed layers. The intermediate layers serve at least two functions in the recording layer. One is to eliminate the exchange-coupling of the SUL and recording layer. If the SUL and recording layer are coupled, the recording media may show larger noise during readback. Another function of the intermediate layer is to provide epitaxial growth conditions for the recording layer. This serves to obtain perpendicular orientation of the recording. Intermediate layers have also been used to decrease the grain size of the recording layer.[33] The recording layer is used to store information and to produce the signal when reading back the information. The disk will then be coated with a carbon overcoat layer will helps to prevent corrosion of the

recording layer. Typically, two types of carbon layers are used: an amorphous carbon layer and a diamond-like carbon (DLC) layer. While both serve to prevent corrosion, the DLC layer also helps in the bonding of the lubricant layer to the disk. The lubricant layer is used to ensure a uniform fly-height of the recording head and to prevent wear and tear on the head, which can cause the head to crash onto the disk.

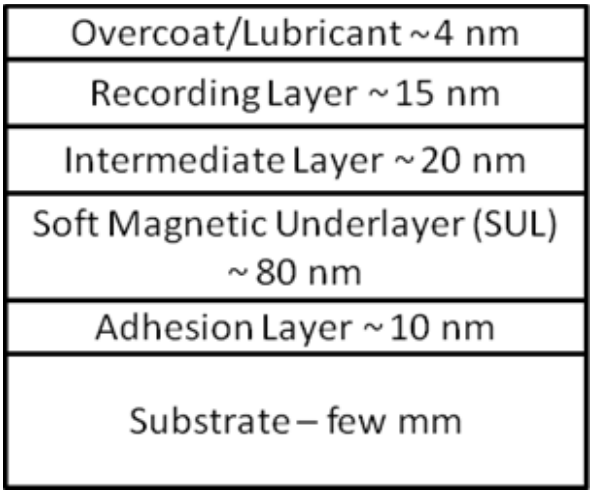

Fig. 6. Different functional layers of perpendicular recording medium with approximate thicknesses (layers not to scale).

2. Soft magnetic underlayers

As discussed earlier, the soft magnetic underlayer in the perpendicular recording media is helpful during the writing of information. It is the presence of a soft magnetic underlayer in the recording media that provides a significant advantage for perpendicular recording technology. With a soft magnetic underlayer and a single-pole head, higher writing fields can be achieved. If higher writing fields are achieved, materials with high K_u can be used as the recording media. Therefore, smaller grains can be used in the recording medium to store information. With stable grains at smaller sizes, higher linear

density could be achieved. Thus, soft magnetic underlayer is a significant part of perpendicular recording technology. The fact that the longitudinal media did not require a soft magnetic underlayer created a handful of new challenges in perpendicular recording, which are described below.

During the fabrication of a recording medium, all the layers discussed except the lubricant are deposited by a sputtering process. The disk substrate (glass or Al-alloy) will pass from one sputtering chamber to another and finally leave the deposition system. During this process, each layer will be sputtered in a sputtering chamber that is isolated from the rest of the chambers. This is to help prevent contamination. The number of disks that can be produced by a system in 1 hour throughput depends on the time that each disk spends in a particular chamber. The deposition of thicker layers needs longer time to sputter, which would reduce the throughput. Thus, by adding an SUL and any seed or intermediate layers that come with it, the manufacturing efficiency is reduced. Another manufacturing problem that would arise because of thicker SULs is that higher deposition rates would be needed, which are usually achieved at higher powers. However, sputtering at higher power would cause spitting of particles, which would deteriorate the surface of the disk and make it unsuitable for the flying heads in a hard disk drive. Therefore, thicker layers are not desirable in the production. In order to avoid these problems, thicker layers are usually deposited in two or three chambers to increase the throughput. This leads to an increase in the number of sputtering stations, which will lead to a significant investment. However, if the performance of perpendicular recording media is justifiably higher, investment will not be of concern. This was one reason why the

industry did not choose perpendicular recording technology for a long time, as the longitudinal recording media provided significant performance and cost advantages.

The fact that the SUL is too thick compared to the recording layer and is also made of materials with a larger magnetization than that of the recording layer also leads to the problem of noise from the SUL. As early as 1984, it was reported that the presence of an SUL, such as Permalloy, can increase the noise from the formation of domains.[34] Soft underlayers are known to contribute to three kinds of noises: spike noise, medium noise, and low noise. Spike noise arises due to the domain walls of the SUL. The medium noise arises from the interaction between the SUL and the residual magnetization of the head. Medium noise is weaker than the spike noise but larger than the low noise.

In the absence of a field, a soft underlayer may form domains, such as stripe domains or 180° domains, as these are ways to minimize the magnetostatic energy. However, the formation of such domain walls would also generate strong magnetic fields, which will cause strong noise during the reading process. A 180° domain wall with the magnetization along the track direction can be considered similar to a transition in longitudinal recording. In longitudinal recording, the signal produced by such a transition will be proportional to its $M_r\delta$. Therefore, if a thick SUL forms a 180° domain wall, the signal produced will be very high. If the domain walls formed in the SUL are fixed in one position, it would be possible to mark that position of the hard disk drive as a bad sector and still use perpendicular recording. However domains that cause spike noise may move from one place to another. Therefore, domain walls are a serious concern. Figure 7 shows MFM images of stripe domains formed in Permalloy thin films[35]. Stripe domain

periodicity is increased due to increasing film thickness. Even though the stripe domains are not as severe as the 180° domains, stripe domains also cause noise during reading.

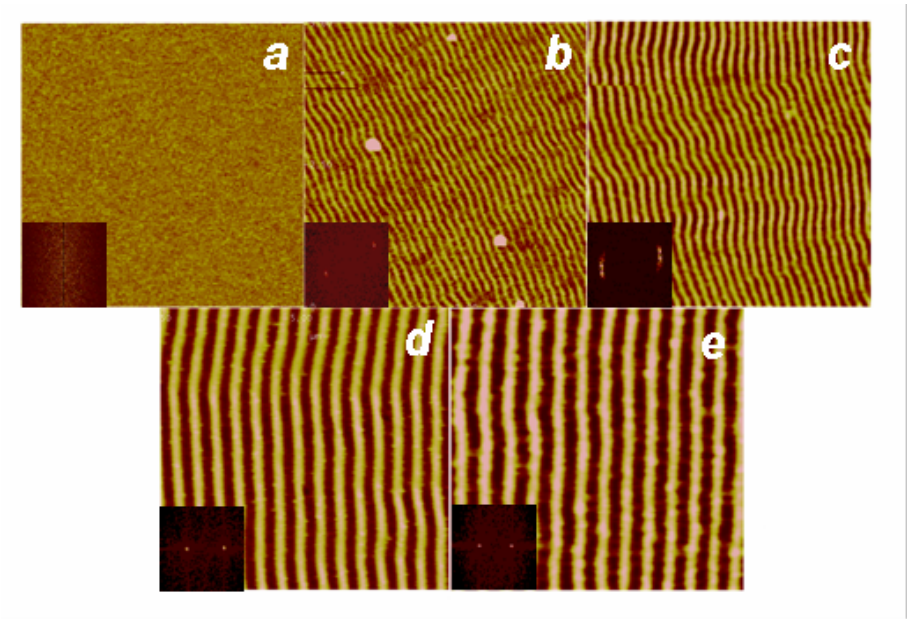

Fig. 7. 5 × 5 μm^2 MFM images of permalloy thin films representing the growth in stripe domain periodicity due to increasing film thickness: (a) lack of stripe domain structures, (b-e) increasing periodicity of stripe domains.

One approach to minimize the noise arising from the SUL is to use new materials that could possibly show fewer domains and hence a lower spike noise. Another approach is to do laminations of SUL material to minimize the domain formation. A third approach is to combine new materials, laminations, and/or processes. However, an easier alternative to reduce the noise of soft magnetic underlayers is to use antiparallelly coupled soft underlayers (APC SUL) through a thin Ru layer. In this case, two or more soft magnetic underlayers could be made to couple to each other anitferromagnetically during the reading, and theoretically the remanances of each layer should cancel each other, as in Figure 8.[1] However, during the writing process, the Zeeman energy would

overcome the antiferromagnetic coupling energy. Therefore, the two layers are aligned in the same direction and would produce a high field during writing.

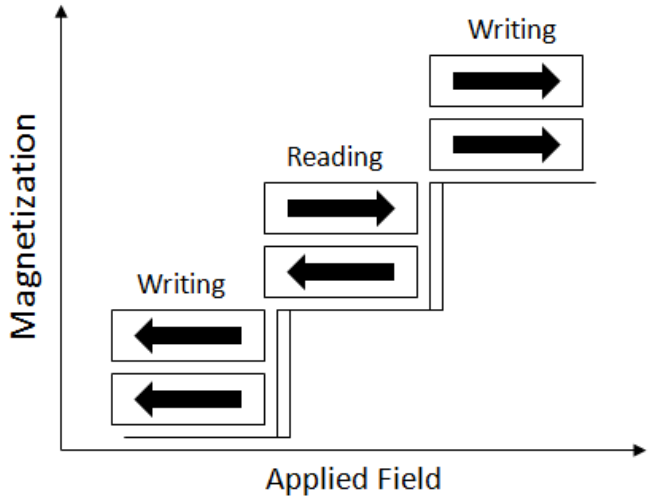

Fig. 8. Magnetization of two layers of anitferromagnetically coupled SUL during the writing and reading.

3. Intermediate layers

When a magnetically soft layer and a hard layer are next to each other, the properties of both the layers would change because of the exchange interaction. Such an exchange interaction could reduce the coercivity of the recording layer and produce a larger noise during the readback. Thus, intermediate layers are inserted between the SUL and recording layer in perpendicular recording as an exchange breaking layer to reduce the noise. However, the exchange breaking intermediate layer must be optimized for use in PMR. If the intermediate layer is too thin, the SUL and recording layer would still be highly exchange coupled. On the other hand, if the intermediate layer is too thick, the SUL would not be able to function properly during the writing process.

Another function of intermediate layers is to induce a perpendicular hcp[002] orientation for the Co-alloy-based recording layer. In Co-alloy-based perpendicular recording media, the easy axis (*c* axis of the hcp crystal) needs to be deposited with a perpendicular orientation with respect to the substrate. In current designs of perpendicular recording media, amorphous materials are considered as the SUL because they could provide lower noise and exhibit a very low average roughness. However, when a Co alloy is deposited directly on top of the amorphous SUL, the hcp(002) texture does not easily develop. Therefore, it is essential to grow intermediate layers that would induce a hcp(002) orientation on the Co-alloy-based recording layer. Recently, intermediate layers have also been loaded with an additional role of producing the right morphology to control the segregation of grains in the recording layer.

4. Recording layers

The material used for the recording layer of perpendicular media has traditionally been a Co alloy. The CoCr alloy was the original media proposed in the late 1970s. Since then, modifications of Co alloys such as CoCrPt, CoCrTa, CoCrNb, CoCrPtNb, and CoCrPtB have been used as the recording layer material.[36-43] One of the major problems of CoCr-alloy media materials was that the nucleation field (field required to switch 5% of the magnetization) of the recording layer was seen in the first quadrant of the hysteresis loop. This implies that at zero fields magnetization of several grains has already reversed. Such grains with reversed magnetization would exhibit a high dc noise. Figure 9 is an illustration to show the significance of nucleation field. The grains are magnetized into the plane of the paper with an applied field. When the field is removed,

all the grains are expected to maintain the magnetization if they are thermally stable and their anisotropy energy is higher than that of the demagnetizing energy. However, if the anisotropy constant of the media is not high, some grains (smaller ones) would reverse, as in Figure 9(a). However, if the anisotropy is high enough, all the grains would maintain their magnetization in the applied field direction, as in Figure 9(b). This could be seen as hysteresis loops with nucleation fields in the first quadrant and second quadrant for media with low K_u and high K_u, respectively [Figures 9(c) and 9(d)]. Therefore, media with high anisotropy are needed to obtain a negative nucleation field. In the earlier days, it was difficult to obtain such media as Cr was used as an additive element to obtain the exchange decoupling. As a side effect, the presence of Cr led to media with lower anisotropy energy.[1]

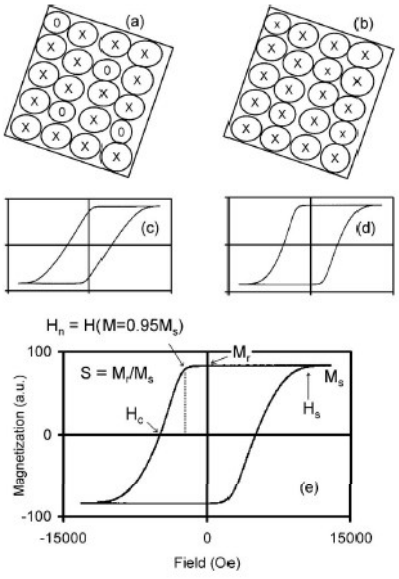

Fig. 9. (Top) Illustration of remanence magnetization state of grains of perpendicular media after it was saturated with a field into the plane. (a) Grains with a lower anisotropy constant show a reversal with remanent magnetization out of the plane showing instability. (b) Grains with a higher anisotropy constant show stable magnetization. (Middle) Illustration of hysteresis loops of the respective media that show (c) a positive H_n and (d) a negative H_n. (Bottom) Hysteresis loop with relevant parameters.

Recently, oxide-based CoCrPt materials have used for perpendicular recording. In these media, CoCrPt is sputtered together with an oxide such as Si-oxide or Cr-oxide. This oxide element can be present in the target or can be formed in the film during the reactive sputtering of the target in an oxygen atmosphere.[44-49] Since Co and the oxide do not mix well, Co alloy grains will be surrounded by an oxide based grain boundary. Because of the oxide material, less Cr is needed to help decouple the Co grains. About 5-10 at. % of Cr is sufficient, as compared to 14-17 at. % of Cr needed in the CoCrPt media without oxides. Morever, in the CoCrPt-oxide media, some of the Cr would oxidize and go to the grain boundary as well. As a result, the grain could have low Cr in its core and therefore a higher anisotropy constant. Such grains would be thermally stable, and a squareness close to one could be achieved. The oxide based grain boundary is also effective in reducing the grain size and in reducing the intergranular exchange interaction. Therefore, the noise can be reduced and sharper transitions are possible. Another advantage of CoCrPt-oxide materials is that the manufacturing process will be more or less the same as that of longitudinal recording media. And, more importantly, small grain size, low noise, and good thermal stability could all be achieved with oxide-based media.

In order to continue the use of CoCrPt-oxide media, it will be necessary to identify suitable oxide materials as the recording layers or other methods that would form a narrow grain boundary but effectively decouple the grains. The new oxide materials should also help in achieving narrower grains and a narrower grain size distribution. The future media would also have need a higher anisotropy constant to overcome the thermal instability issues by reducing the Cr content or by increasing the Pt content. Reducing the

grain size and distribution of the existing CoCrPt-oxide media using other methods is also possible.

C. The Future of Magnetic Recording

In today's data storage industry, perpendicular magnetic recording has already achieved areal densities beyond 600 Gbits/in^2. Some experts predict that with current materials, PMR can achieve recording densities up to 1 Tbits/in^2 within the next 5 years if current advancements persist. However, beyond 1 Tbits/in^2, CoCrPt-oxide perpendicular media, as with longitudinal media, will begin to reach the superparamagnetic limit, that is, when thermal fluctuation of the magnetic grains within bits occurs at room temperature.[50] This instability results from the volume size of the magnetic grains becoming too small. In order to achieve recording densities beyond 1 Tbits/in^2, new materials must be developed. One such material that has the potential to support high-density perpendicular recording is highly anisotropic FePt. It has a high magnetocrystalline anisotropy ($K_u \sim 10^8$ ergs/cm^3) allowing for grain sizes of only a few nanometers while maintaining good thermal stability.[51,52] When FePt thin films are deposited at room temperature, the crystal structure is an fcc phase that does not exhibit a high anisotropy. However, when annealed (or heated during deposition) at temperatures greater than 400 °C, the highly anisotropic fct-FePt is formed. This phase is commonly known as the $L1_0$-phase. $L1_0$-ordered FePt thin films are a promising candidate for the future of magnetic recording because of their excellent material properties. Not only is $L1_0$-FePt seen as a potential candidate for future PMR devices, but for next-generation storage devices as well. The next two sections will present the results of $L1_0$-FePt research for future use as a perpendicular magnetic

recording material. The following three sections will present research on $L1_0$-FePt for possible next-generation storage devices to increase areal densities beyond 1 Tbits/in^2 with theoretical storage densities greater than 10 Tbits/in^2. The future technologies to be discussed are discrete track/bit-patterned media, heat assisted magnetic recording and 3-D magnetic recording.

IV. Microstructural Enhancement of FePt Thin Films

$L1_0$-ordered FePt has received much attention since its proposal as an ultrahigh density magnetic recording material due to its large uniaxial magnetic anisotropy (7×10^7 ergs/cm^3).[52] Several underlayers have been investigated in order to induce perpendicular orientation[53-60], as well as reduce the $L1_0$ ordering temperature.[61-65] Also, several methods and materials have been investigated in order to reduce the grain size[66-73] of the FePt films, as grain sizes of less than 6 nm are necessary for ultrahigh density magnetic recording.[74] However, little research has been done to improve the roughness of $L1_0$ FePt films. Surface roughness is crucial to the magnetic recording industry because the fly height of the write/read head for advanced technologies is approximated to be less than 2 nm.[75] If the surface of the media is too rough, this will cause either an increase or decrease in the fly height of the write/read head. In the case where the fly height is increased, this will lead to a reduced magnetic field coming from the write head, potentially making the media unwritable. In the case where the fly height is decreased, the head can come into contact with the surface of the media, thus causing the head to crash and rendering the whole device useless. In this work, the roughness, as well as the

magnetic and structural properties, of FePt films was studied in relation to the initial substrate conditions.

A. Experiment

Four sets of samples were fabricated on Si, SiO_2 (300 nm thick SiO_2 on Si) and glass substrates using different initial substrate conditions. The first set of samples was prepared with the structure of substrate/$Cr_{90}Ru_{10}$/MgO/$Fe_{55}Pt_{45}$ (no Ar milling, no Ta). The second set of samples was prepared with the structure of substrate/$Cr_{90}Ru_{10}$/MgO/$Fe_{55}Pt_{45}$, with substrate Ar-ion milling performed before film deposition (with Ar milling, no Ta). The third set of samples was prepared with the structure of substrate/Ta/$Cr_{90}Ru_{10}$/MgO/$Fe_{55}Pt_{45}$ (no Ar milling, with Ta). The last set of samples was prepared with the structure of substrate/Ta/$Cr_{90}Ru_{10}$/MgO/$Fe_{55}Pt_{45}$, with substrate Ar-ion milling performed before film deposition (with Ar milling, with Ta). The films were prepared by dc or rf magnetron sputtering with a base pressure below 1×10^{-7} Torr. The Ta adhesion layer was deposited at room temperature (RT) with a processing pressure of 10 mTorr and a thickness of 2.5 nm. The CrRu underlayer was deposited at 300 °C under 3 mTorr processing pressure and a thickness of 25 nm. The MgO interlayer was deposited at 90 °C with a processing pressure of 5 mTorr and a thickness of 6 nm. The FePt layer was deposited at 550 °C with a processing pressure of 10 mTorr and a thickness of 5 nm. The temperature of each layer was held for 15 minutes before sputtering in order to ensure temperature equilibrium. The Ar-ion milling was performed with 5 mTorr Ar pressure and 25 W rf power for 2.5 minutes, the time and power

required to remove the native-SiO_2 layer from the Si substrate. The magnetic properties were measured with a polar magneto-optical Kerr effect (MOKE) system. Structural properties were measured via x-ray diffraction (XRD) while the thin films' microstructure was measured using atomic force microscopy (AFM). The AFM analysis was performed in tapping mode with scan sizes of 5×5 μm^2 and 1.5×1.5 μm^2.

B. Results and Discussion

For areal densities of 1 Tbit/in.^{2}, the required lowest coercivity is 1.2 Tesla.[76] Therefore, it is crucial to maintain high coercivity FePt thin films while reducing the surface roughness. Figure 10 shows the out-of-plane hysteresis loops of the FePt thin films deposited at different substrate conditions. Samples deposited on substrates after Ar-ion milling showed much larger coercivity (H_c) than samples without Ar-ion milling. Samples with Ar-ion milling exhibited H_c values greater than 2 Tesla, whereas samples without Ar-ion milling showed H_c values between 0.4-1.6 Tesla. For samples deposited on Si substrates, this increase in H_c is due to the Ar-ion milling removing the native-SiO_2 layer, thus, enabling better adhesion and (200) growth of the CrRu layer. For SiO_2 and glass substrates, the increase in H_c can be attributed to the Ar-ion milling removing any particles or contaminants, allowing for the CrRu layer to be deposited on a much cleaner surface. There is also a slight increase in H_c with the samples without Ar-ion milling when Ta is used due to the Ta serving as an adhesion layer between the CrRu layer and the substrates.

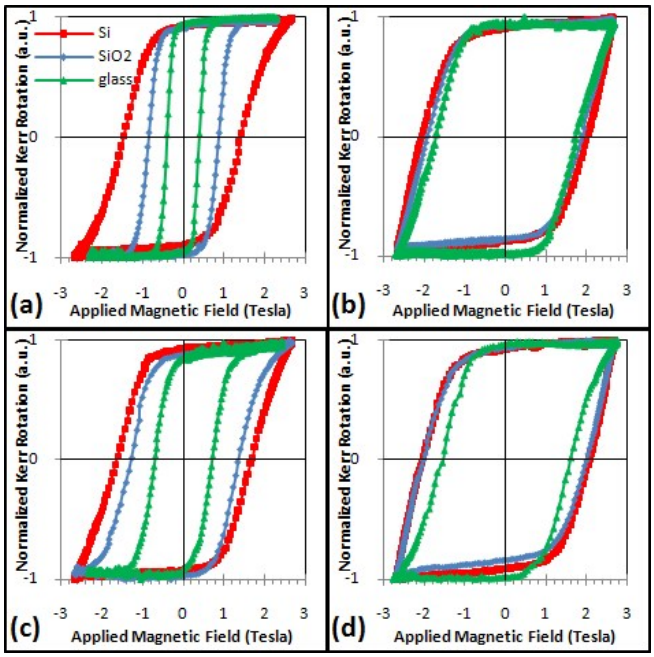

Fig. 10. Out-of-plane hysteresis loops of FePt films on Si, SiO_2 and glass substrates using (a) no Ar milling, no Ta (b) Ar milling, no Ta (c) no Ar milling, with Ta and (d) Ar milling, with Ta. Note: legend in (a) also applies to (b)-(d).

Figure 11 shows the XRD spectra of the FePt thin films deposited on Si, SiO_2, and glass substrates using various initial substrate conditions. For all three different substrates, the best crystallographic conditions were observed on the samples deposited on substrates with Ar-ion milling and without Ta adhesion layer, as evidenced by the highest FePt (001) and CrRu (200) peaks. However, for Si, the second-best crystallographic conditions came from the sample deposited with Ar-ion milling and Ta adhesion layer, whereas for SiO_2 and glass substrates the second-best crystallographic conditions came from samples without Ar-ion milling and no Ta adhesion layer. For Si substrates, this states the importance of removing the native-SiO_2 layer before the deposition of the CrRu layer. For SiO_2 and glass substrates, this shows that a Ta adhesion layer can actually be detrimental to the (200) growth of the CrRu layer.

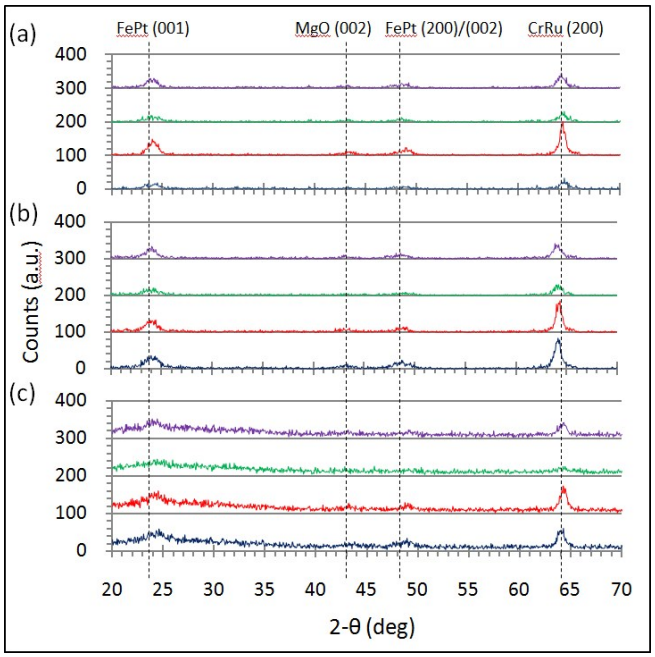

Fig. 11. XRD spectra of FePt films on (a) Si, (b) SiO_2, and (c) glass substrates using (from bottom to top): no Ar milling, no Ta; Ar milling, no Ta; no Ar milling, with Ta; Ar milling, with Ta.

Figures 12 - 14 show the 1.5 × 1.5 μm^2 AFM images for Si [Figure 12], SiO_2 [Figure 13], and glass [Figure 14] substrates that have been deposited with different initial substrate conditions. Relatively larger in-plane surface roughness emerged for the Si substrate sample deposited without Ar-ion milling and without Ta adhesion layer. This is due to the poor adhesion between the native-SiO_2 of the Si substrate and the CrRu layer. During deposition of the FePt layer, the sample is heated to 550 °C which causes the CrRu layer to become extremely rough, developing peaks and valleys as seen in Figure 12(a). This point is further exemplified with Figure 15, which shows the 2-D power spectral densities (PSD) of the samples in Figure 12, along with a 25 nm CrRu layer deposited on Si without Ar-ion milling and without Ta, then heated at 550 °C for 15 minutes. While the in-plane surface roughness wavelengths of Figures 12(b-d) diminished for wavelengths above 50 nm, both the sample in Figure 12(a) and the CrRu

sample exhibited a significant increase in PSD for wavelengths between 50 nm and 2 μm. Hence, the cause of the large roughness in Figure 12(a) is due to poor adhesion between the CrRu and native-SiO_2 layers when the sample is heated to 550 °C during the FePt deposition. This issue can be readily solved by the use of Ar-ion milling on the Si substrate, or the use of a Ta adhesion layer, or both. However, according to the XRD spectra in Figure 11, the use of a Ta adhesion layer is detrimental to the (200) growth of the CrRu layer. Therefore, for best results, only the Ar-ion milling should be used. For the SiO_2 and glass substrates, the surface roughness was below 1 nm for all four initial substrate conditions, which is suitable for magnetic recording. However, as with the Si substrates, the used of a Ta adhesion layer caused a decrease in the (200) CrRu peak.

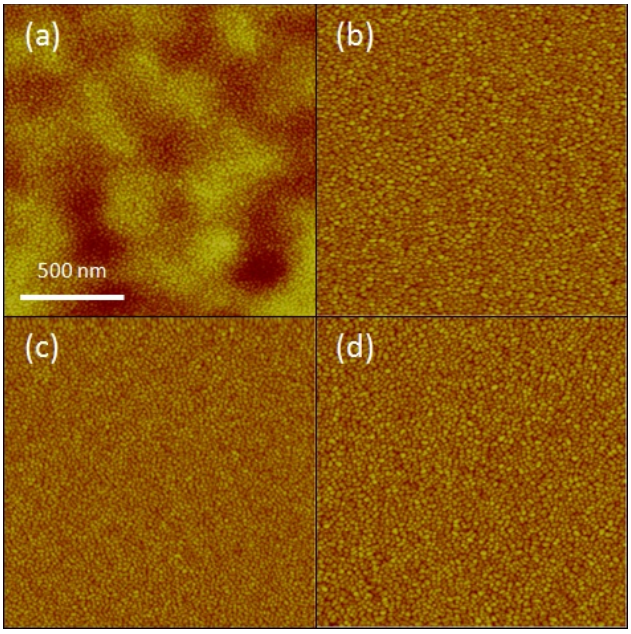

Fig. 12. 1.5 × 1.5 μm^2 AFM images of FePt thin films using (a) no Ar milling, no Ta; (b) with Ar milling, no Ta; (c) no Ar milling, with Ta; and (d) with Ar milling, with Ta deposited on Si substrates with a data scale of 20 nm.

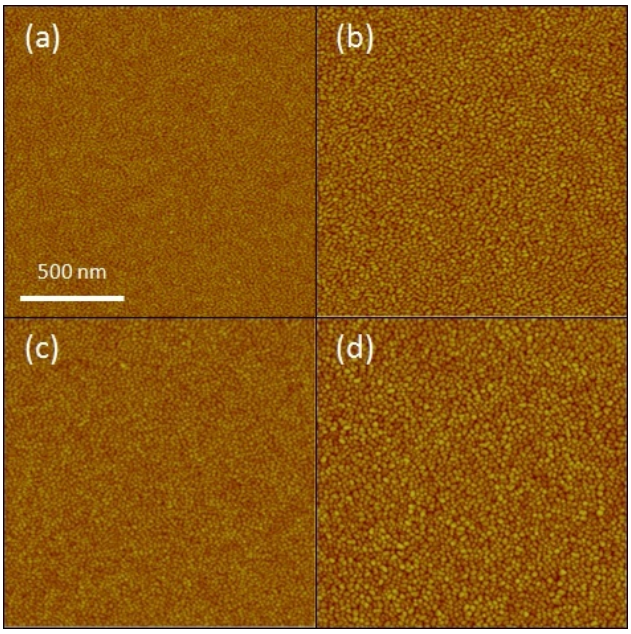

Fig. 13. 1.5 × 1.5 μm^2 AFM images of FePt thin films using (a) no Ar milling, no Ta; (b) with Ar milling, no Ta; (c) no Ar milling, with Ta; and (d) with Ar milling, with Ta deposited on SiO_2 substrates with a data scale of 20 nm.

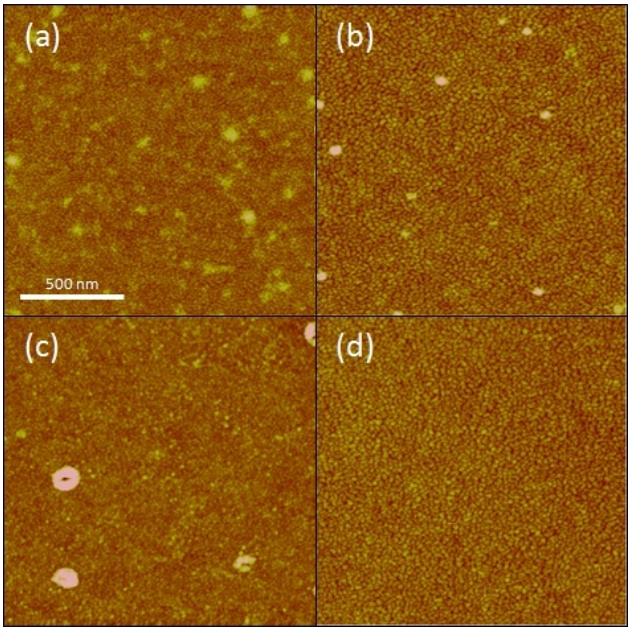

Fig. 14. 1.5 × 1.5 μm^2 AFM images of FePt thin films using (a) no Ar milling, no Ta; (b) with Ar milling, no Ta; (c) no Ar milling, with Ta; and (d) with Ar milling, with Ta deposited on glass substrates with a data scale of 20 nm.

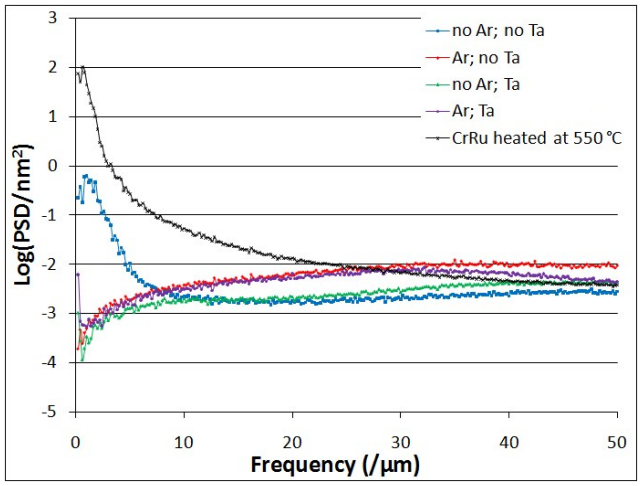

Fig. 15. 2-D power spectral densities for the first set of samples deposited on Si substrates along with a sample of 25 nm CrRu deposited without Ar milling or Ta and heated at 550 °C for 15 minutes.

C. Conclusion

The effects of substrate Ar-ion milling and Ta adhesion layer on the microstructural and magnetic properties of $L1_0$-FePt thin films were investigated. The large in-plane surface roughness of the FePt films deposited on Si substrates was concluded to be due to poor adhesion between the native-SiO_2 and the CrRu layers. The issue was resolved by the use of substrate Ar-ion milling before deposition and/or the use of a Ta adhesion layer. However, for all three substrates, the use of a Ta adhesion layer was shown to be detrimental to the (200) growth of the CrRu layer and the largest coercivity was obtained from the samples grown exclusively with Ar-ion milling. To conclude, FePt films with coercivity field values higher than 2 Tesla and out-of-plane roughness (R_a) less than 1 nm were fabricated, showing both the importance of substrate Ar-ion milling and the feasibility of FePt films as a next-generation magnetic recording media.

V. Optimizing the Sputter Parameters of FePt Thin Films

$L1_0$-ordered FePt thin films are a leading candidate for next-generation magnetic recording, such as bit-patterned media (BPM)[77], heat-assisted magnetic recording (HAMR)[78], and multilevel three-dimensional (ML3D) magnetic recording[79], because of their excellent material properties. Its high magnetocrystalline anisotropy of ~ 10^8 ergs/cm^3 allows for grain sizes less than a few nanometers while maintaining good thermal stability[80]. It also has been demonstrated that $L1_0$-FePt can achieve coercivity greater than 10 Tesla[81]. However, in order to achieve the $L1_0$-phase requires post-annealing and/or deposition at elevated substrate temperature. Several underlayers have been investigated that can reduce both the ordering temperature and the in-plane contributed variant, thus accelerating the ordering transformation temperature and inducing the (001) preferred orientation[82-93]. In this work, the effects of sputtering pressure, sputtering temperature, and thickness of the FePt layer, as well as the thicknesses of the underlayers on the structural and magnetic properties of FePt thin films have been investigated in order to optimize the sputtering process of high coercivty FePt thin films.

A. Experiment

Five FePt thin film series were prepared on silicon substrates with a base pressure better than 1×10^{-7} Torr. Table I shows the film structure of each series, along with the parameter investigated in each series. The sputter powers were 115 W dc for CrRu, 270 W rf for MgO and 75 W dc for FePt. The CrRu layer was deposited with 3 mTorr working pressure at 300 °C and the MgO layer was deposited with 5 mTorr working

pressure at 90 °C for all series. The FePt layer was deposited with different working pressure for Series I, and with 10 mTorr working pressure for Series II-V. The FePt sputter temperature was 550 °C for Series I and III-V and was varied for Series II. The FePt layer was deposited using a $Fe_{55}Pt_{45}$ composite target, which resulted in a $Fe_{50}Pt_{50}$ composition determined by energy dispersive x-ray (EDX) analysis. The crystallographic texture of the films was examined with x-ray diffraction (XRD) and the surface roughness was measured using atomic force microscopy (AFM). The magnetic properties were measured with magnetic force microscopy (MFM) and with a magneto-optical Kerr effect (MOKE) system with a field range of ± 2.7 Tesla.

Table I. Film structure of each series and the parameter investigated in each series of samples.

Series	Film Structure	Parameter
I	$Cr_{90}Ru_{10}$(25 nm)/MgO(6 nm)/$Fe_{50}Pt_{50}$(5 nm)	FePt Pressure
II	$Cr_{90}Ru_{10}$(25 nm)/MgO(6 nm)/$Fe_{50}Pt_{50}$(5 nm)	FePt Temperature
III	$Cr_{90}Ru_{10}$(25 nm)/MgO(6 nm)/$Fe_{50}Pt_{50}$(2-16 nm)	FePt Thickness
IV	$Cr_{90}Ru_{10}$(0-25 nm)/MgO(6 nm)/$Fe_{50}Pt_{50}$(5 nm)	CrRu Thickness
V	$Cr_{90}Ru_{10}$(25 nm)/MgO(2-6 nm)/$Fe_{50}Pt_{50}$(5 nm)	MgO Thickness

B. Results and discussion

1. FePt Sputter Pressure

Figures 16 and 17 show the out-of-plane hysteresis loops and XRD spectra of the FePt films in Series I, respectively. The samples sputtered at 10 and 15 mTorr gave the highest coercivity, 1.75 Tesla, while the sample sputtered at 25 mTorr gave the lowest coercivity, 1.05 Tesla. The sample sputtered at 5 mTorr resulted in a coercivity of 1.45 Tesla. While the FePt (001) peak of all four samples are almost identical, the FePt

(200)/(002) peaks of the samples sputtered at 10 and 15 mTorr appear to be much sharper than those sputtered at 5 and 25 mTorr, which may contribute to the higher coercivity values. Figure 18 shows the surface roughness and sputter rate of the FePt films sputter at different working pressure. As the sputter pressure increases, so does the surface roughness. Since the sputter rate increased from 5 to 10 mTorr, then decreased from 10 mTorr to 25 mTorr, the surface roughness can be is dependent on the sputter pressure and not the sputter rate. From the MFM images in Figure 19, it was determined that the sputter pressure has no affect on the magnetic domain size.

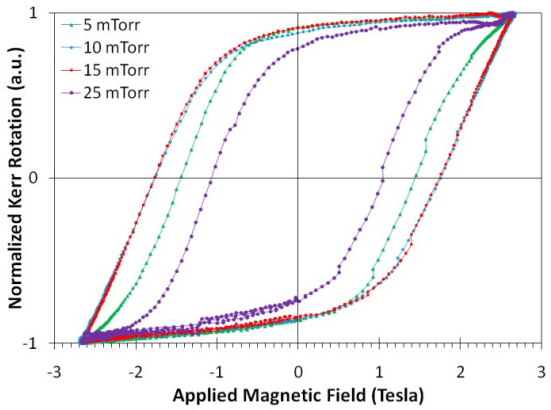

Fig. 16. Out-of-plane hysteresis loops of Series I FePt films with the FePt layer sputtered at different working pressure.

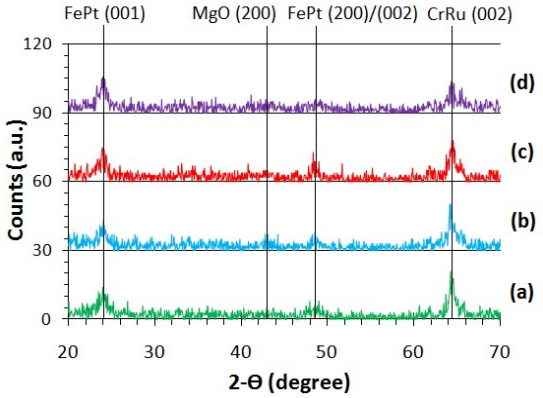

Fig. 17. XRD spectra of Series I FePt films with FePt working pressure of (a) 5 mTorr, (b) 10 mTorr, (c) 15 mTorr, and (d) 25 mTorr.

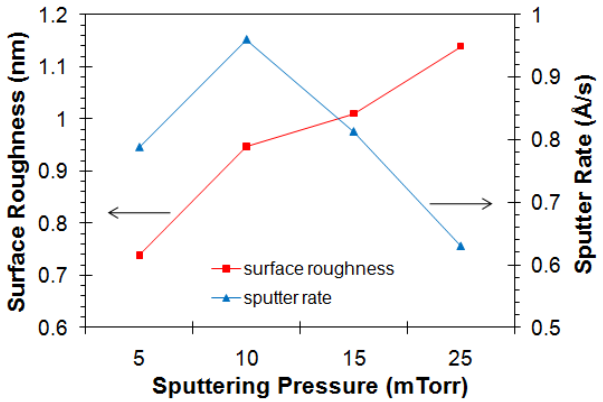

Fig. 18. Surface roughness and sputter rate of Series I FePt films with the FePt layer sputtered at different working pressure.

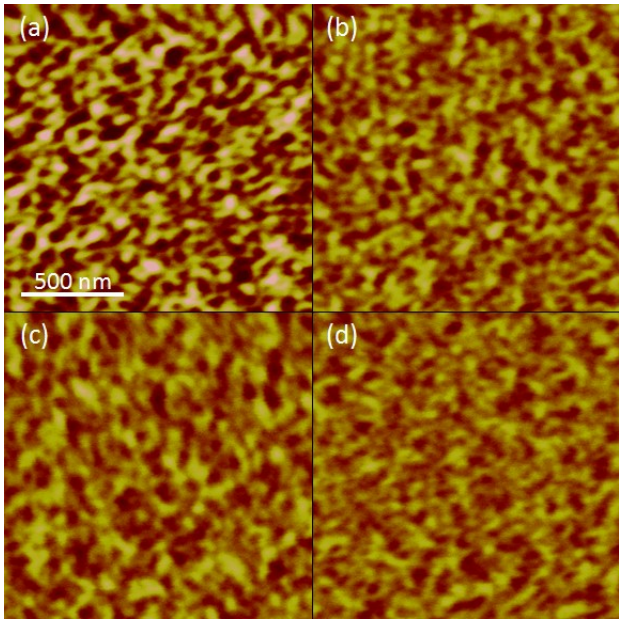

Fig. 19. 1.5 μm × 1.5 μm MFM images of Series I FePt films with the FePt layer sputtered at (a) 5 mTorr, (b) 10 mTorr, (c) 15 mTorr, and (d) 25 mTorr, all with phase of 4°.

2. FePt Sputter Temperature

Figures 20 and 21 show the out-of-plane hysteresis loops and XRD spectra of the FePt films in Series II, respectively. From the XRD analysis, the FePt (001) peak is observed even at 350 °C. At this temperature the hysteresis loop show good squareness

and perpendicular magnetization, however, the coercivity is only 0.4 Tesla. When the FePt layer is sputtered at 450 °C the coercivity increases to 1.2 Tesla. A further increase in temperature results in coercivity values of 1.75 and 1.85 Tesla, when sputtered at 550 °C and 650 °C, respectively. Interestingly, the CrRu (002) becomes much broader and less intense as the samples are heated with higher temperature values. This demonstrates that heating the samples at higher temperatures can deteriorate the CrRu (002) texture.

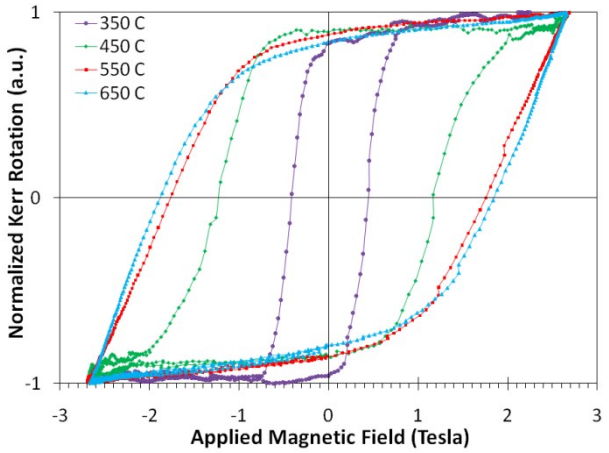

Fig. 20. Out-of-plane hysteresis loops of Series II FePt films with the FePt layer sputtered at different temperatures.

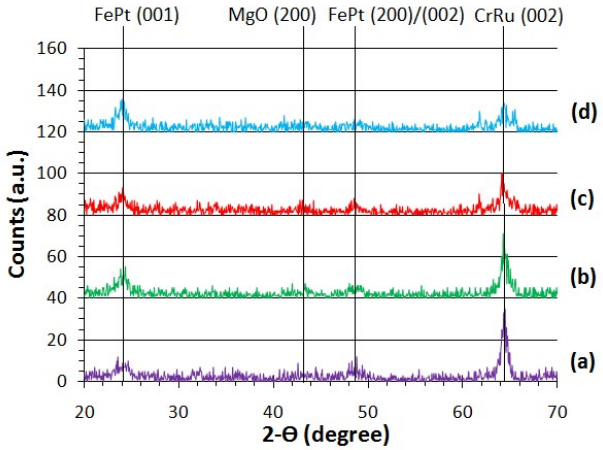

Fig. 21. XRD spectra of Series II FePt films with the FePt layer sputtered at (a) 350 °C, (b) 450 °C, (c) 550 °C, and (d) 650 °C.

3. FePt Thickness

In ML3D magnetic recording, the magnetic moment of each recording layer should be at least twice that of the recording layer above it. This ensures that some of the generated magnetic signals are not canceled out when the magnetic layers are magnetized in opposite directions, allowing for each recording layer to generate a distinguishable read-back signal.[79] For this reason, the FePt thicknesses in Series III were chosen as 2, 4, 8, and 16 nm. The out-of-plane hysteresis loops and XRD spectra of Series III are shown in Figures 22 and 23, respectively. The data for 5 nm FePt thickness from Series I and II was also added for this comparison. For thicknesses between 4-8 nm, the FePt films show coercivity values greater than 1.8 Tesla. However, when the thickness is increased to 16 nm, the coercivity drops to 1.4 Tesla. When the FePt thickness is only 2 nm, the magnetostriction causes the easy-axis magnetization of the film to be in-plane, as demonstrated by the positive nucleation field, H_n, of the hysteresis loop. This is further demonstrated by the MFM images in Figure 24, where the magnetic domain boundaries are less defined in Fig. 24(a) than in Fig. 24(b)-(d).

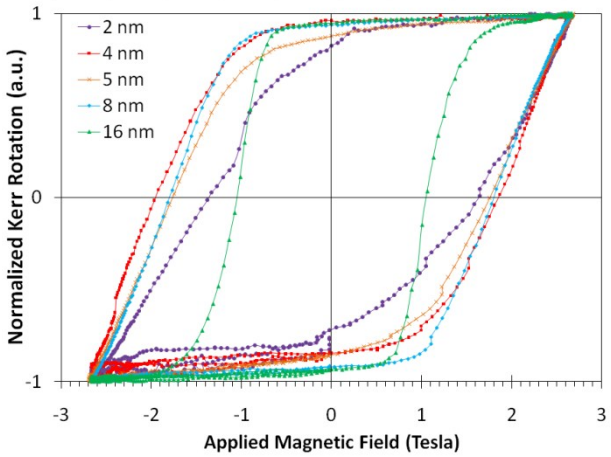

Fig. 22. Out-of-plane hysteresis loops of Series III FePt films with various FePt layer thicknesses.

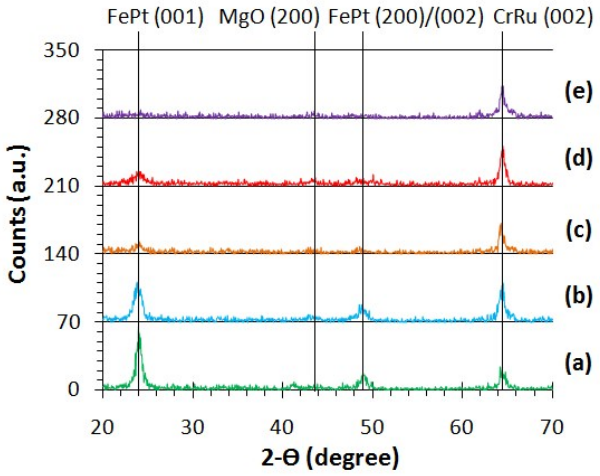

Fig. 23. XRD spectra of Series III FePt films with FePt thickness of (a) 16 nm, (b) 8 nm, (c) 5 nm, (d) 4 nm, and (e) 2 nm.

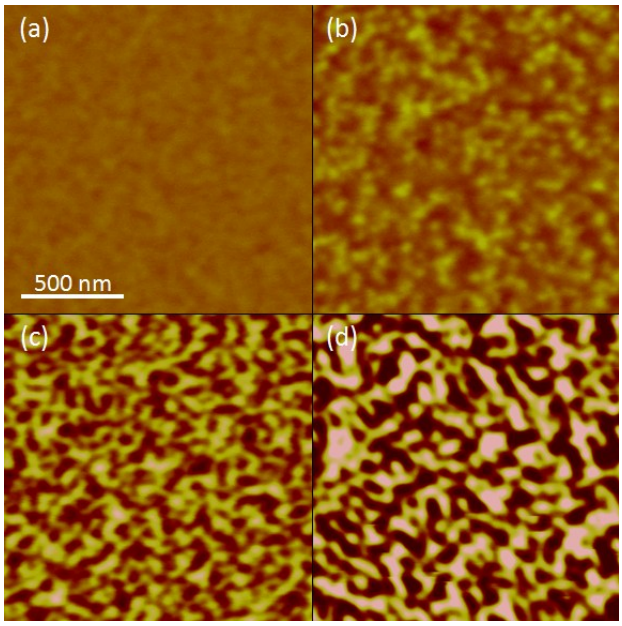

Fig. 24. 1.5 μm × 1.5 μm MFM images of Series III FePt films with FePt thickness of (a) 2 nm, (b) 4 nm, (c) 8 nm, and (d) 16 nm, all with a phase of 8°.

4. Underlayer Thickness

Figure 25 shows the out-of-plane hysteresis loops for Series IV FePt films with varying CrRu underlayer thicknesses while Figure 26 shows the out-of-plane hysteresis loops for Series V FePt films with varying MgO interlayer thickness. FePt films with a

CrRu underlayer thickness of 5 nm exhibits similar coercivity (1.1 Tesla) to that of FePt films grown without a CrRu underlayer. However, FePt films with a coercivity of 1.8 Tesla were achieved on a 10 nm CrRu layer, which is remarkable considering previous $L1_0$-FePt films have only been achieved on a CrRu underlayer of 30 nm or greater[94-98]. Since the MgO thickness has no effect on the coercivity of the FePt films, it is possible to grow FePt thin films with a coercivity of 1.8 Tesla on only a 12 nm underlayer (10 nm CrRu plus 2 nm MgO). For perpendicular recording that utilizes a soft underlayer (SUL), the magnetic flux travels from the recording head through the media into the soft underlayer and then back to the recording head, as illustrated by Figure 27. Therefore, it is crucial to minimize the gap thickness between the write pole and the SUL, since it is known that decreasing the gap thickness will increase the maximum achievable field, or will decrease the amount of current necessary to obtain maximum field[99-103]. If we assume a FePt thickness of 5 nm, a MgO thickness of 2 nm, and a fly height of 2 nm, then by decreasing the CrRu layer from 30 nm to 10 nm, the total gap thickness will decrease by over a factor of 2.

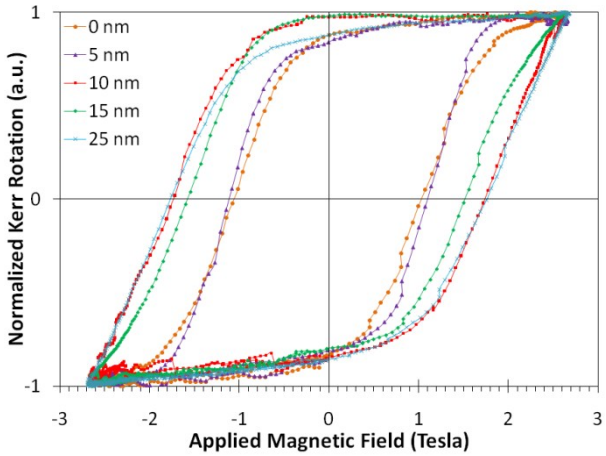

Fig. 25. Out-of-plane hysteresis loops of Series IV FePt films with different CrRu underlayer thicknesses.

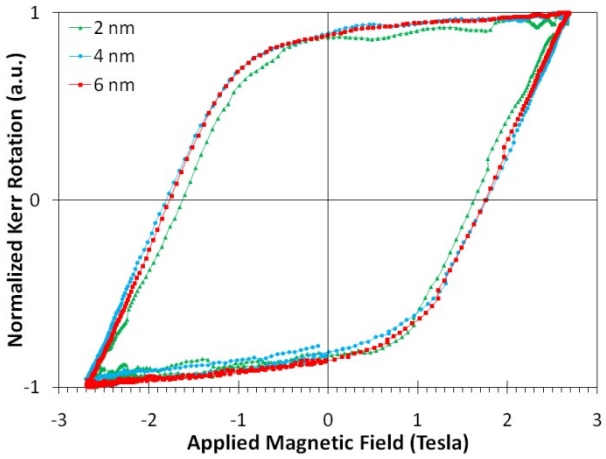

Fig. 26. Out-of-plane hysteresis loops of Series V FePt films with different MgO interlayer thicknesses.

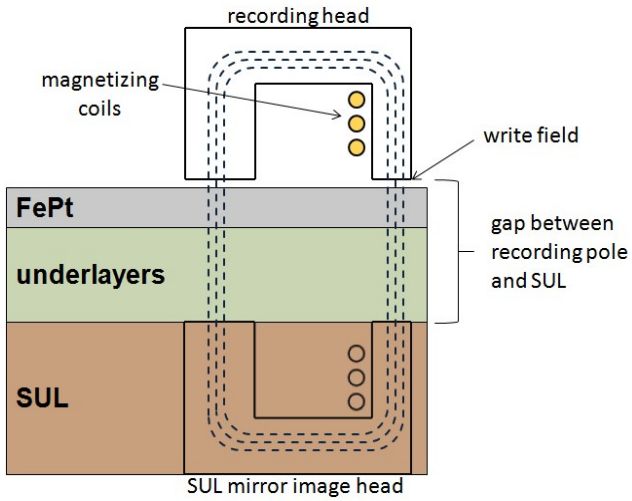

Fig. 27. A simple schematic of a perpendicular magnetic recording process on a FePt thin film with a soft underlayer.

4. Conclusion

The magnetic and microstructural properties of FePt thin films were investigated by varying the FePt sputter pressure and temperature, as well as the thicknesses of the FePt, MgO, and CrRu layers. It was shown that as the FePt sputter pressure increases, so does the surface roughness (Series I). Although $L1_0$ transformation occurred at 350 °C,

higher sputter temperatures exhibited higher coercivities (Series II). Series III showed that for FePt films, there is a minimum (4 nm) and maximum (8 nm) thickness for obtaining large coercivity films with out-of-plane magnetization. Series IV and V demonstrated that only a 12 nm seed layer is necessary to achieve FePt thin films with coercivity greater than 1.8 Tesla, demonstrating FePt films as a promising candidate for next-generation magnetic recording media.

VI. Bit-Patterned FePt Media Using Pre-Patterned Substrates

As the areal density of hard disks drives become larger and larger, the magnetic bits become smaller and smaller. This leads to greater instability of the bits and lower signal-to-noise (SNR) during readback. This is because as the bits get smaller, the bit surface area touching neighboring tracks becomes larger in relation to the volume of the bit. One approach to maintaining high SNR while reducing adjacent track erasure is discrete track media[104-112] (DTM) and bit-patterned media[109-115] (BPM). In DTM, the tracks (one row of bits) are physically separated from each other through lithography, etching, or other processes. This helps in alleviating some of the SNR and demagnetization issues of the bits from the vertical direction. BPM takes this technology one step further by physically separating the bits in both the vertical and horizontal direction, so that every single bit does not touch one another. In this paper, BPM using high coercivity $L1_0$-FePt as the magnetic material was fabricated. However, since FePt media requires high deposition temperatures and has large fringing fields due to the high coercivity, a new method of fabricating BPM was used. Instead of depositing the

magnetic film and then patterning the thin film, the substrates were patterned first, and after deposition of the FePt layer the patterns still remained.

A. Experiment

The process flow for the pre-patterned substrates is shown in Figure 28. First, PMMA resist was spun coated on Si substrates with a 300 nm SiO_2 layer grown on top. Next, e-beam lithography was performed and then developed leaving the patterns in the photoresist. A thin layer of Cr was deposited and lift-off was performed, which removes the PMMA and leaves small Cr islands on the substrate. These Cr islands are what preserve the patterns during the next step, SiO_2 milling. After SiO_2 milling, another solution is used that dissolves away the Cr but does not affect the SiO_2. This leaves a pre-patterned substrate for depositing the magnetic thin film. The patterns were cylindrical in shape with an average of 45 nm height, with different radii and pitch for comparative analysis.

The magnetic film was deposited with the structure of substrate/MgO (4 nm)/FePt (5 nm). The seed layer and magnetic layer were deposited with the thinnest layers possible so that the film will retain the patterning. The MgO layer was deposited using rf sputtering with 5 mTorr processing pressure at 90° C. The FePt layer was deposited using dc sputtering with 10 mTorr processing pressure at 550° C. The magnetic properties were measured using a Polar Kerr system with an applied field of ±2.7 Tesla. Atomic force microscopy (AFM) and magnetic force microscopy (MFM) was performed on the sample to measure the size, shape and magnetic orientation of the individual patterns.

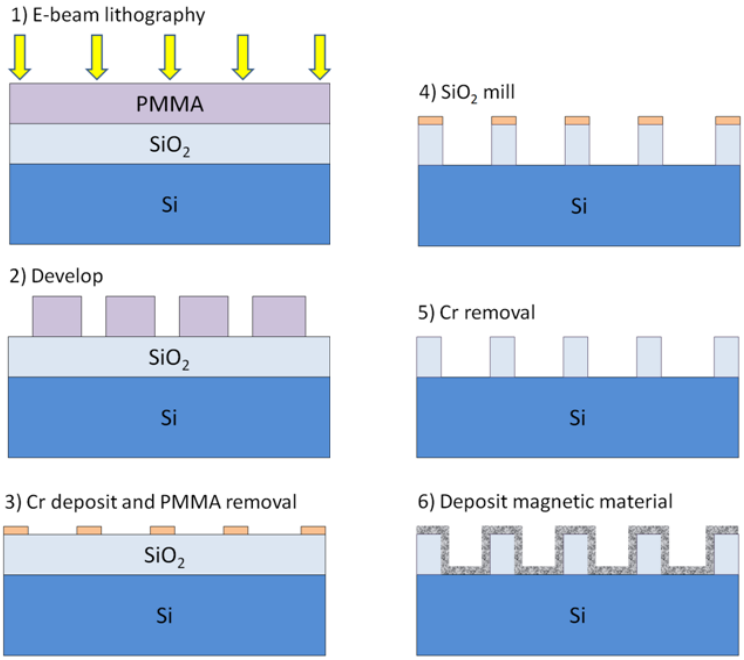

Fig. 28. Schematic process flow for fabricating pre-patterned substrates for bit-patterned media.

B. Results and Discussion

Figure 29 shows 5 µm × 5 µm AFM and MFM images of a set of FePt patterns. The columns were measured to have a diameter of 100 nm with a pitch size of about 150 nm. The pitch is measured as the distance from the center of one column to the center of the other column, so that the actual spacing between the edges of the columns is only 50 nm. The white circles represent where one column is magnetized in the "down" direction (red color) while the black circles show when the column is magnetized in the "up" direction (yellow color). Some columns are partially red and partially yellow, this is due to the size of the column being so large, that the column does not act as a single bit but rather two or more bits. Another reason for this is that some of the bits may not be orientated in the perpendicular direction, but rather some angle in between perpendicular

and horizontal. This is also show in the hysteresis loop, as show in Figure 30 where the squareness of the loop shows the film might be isotropic. Figure 30 also shows that the coercivity of the film is approximately 1.2 Tesla.

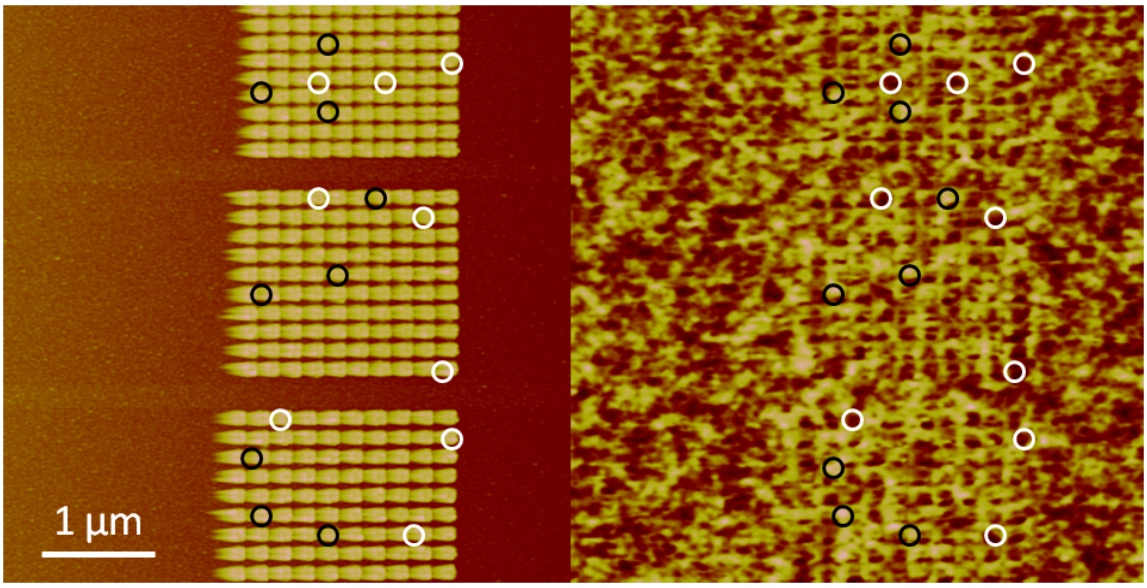

Fig. 29. 5 µm × 5 µm AFM and MFM images of the FePt thin film deposited on pre-patterned substrates. The white circles represent where the individual islands are magnetized in the "down" direction, while the black circles represent where the islands are magnetized in the "up" direction.

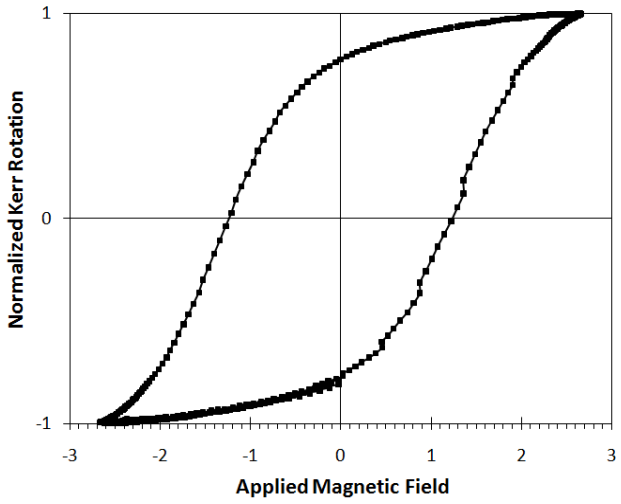

Fig. 30. Out-of-plane hysteresis loop of the patterned FePt thin film.

Figure 31 shows 1 μm × 1 μm AFM and MFM images of a set of FePt patterns with column diameter of 50 nm and a pitch size of 80 nm. Again, the white and black circles represent where the columns are magnetized in the "down" and "up" directions, respectively. In the MFM image, it can be seen that some individual columns are magnetized either "up" or "down" perpendicularly, however, due to the large fringing fields of the high coercivity films, there appear to be "cloud-like" regions above the patterns.

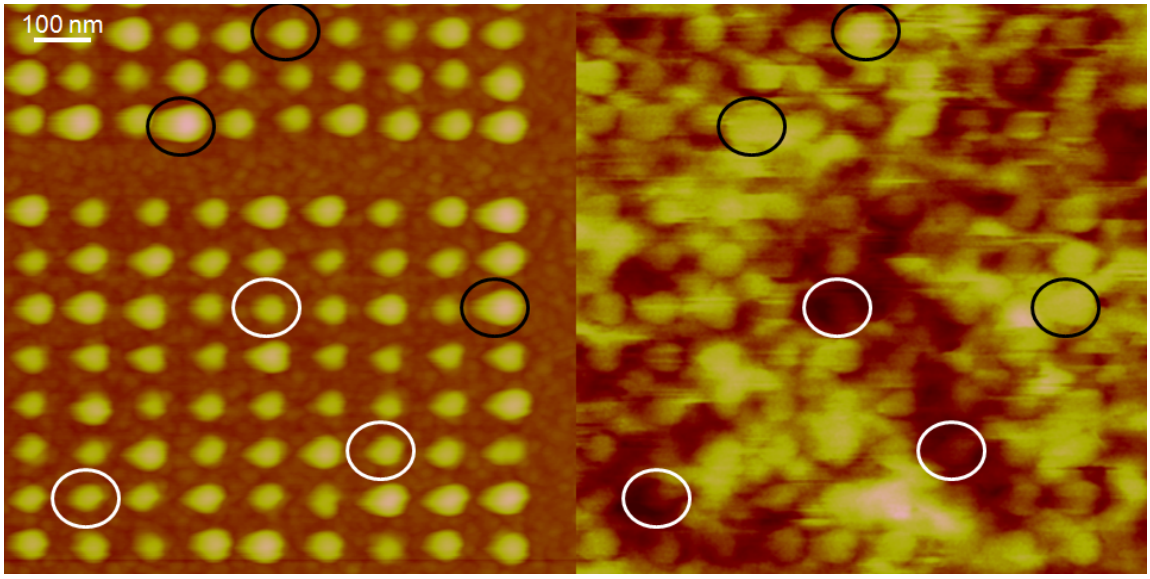

Fig. 31. 1 μm × 1 μm AFM and MFM images of the FePt thin film deposited on pre-patterned substrates. The white circles represent where the individual islands are magnetized in the "down" direction, while the black circles represent where the islands are magnetized in the "up" direction.

C. Conclusion

A new method of fabricating BPM was developed using pre-patterned substrates so that FePt, a relatively new, but intriguing magnetic material could be used in BPM. SiO_2 substrates were patterned first before depositing a FePt film with a coercivity of 1.2

Tesla. Columns of 100 nm and 50 nm diameters were measured and perpendicular orientation of some of these columns was observed. It was shown that a pre-patterned process could be used to develop BPM when conventional methods cannot due to thin film deposition conditions.

VII. Heat-Assisted Magnetic Recording

Heat-assisted magnetic recording (HAMR) has the potential to increase the areal density beyond the limitations of conventional perpendicular magnetic recording.[116,117] In HAMR, the recording media is heated near its Curie temperature during the writing process and needs to cool down quickly to avoid thermal destabilization of adjacent tracks. Furthermore, the bit transition length depends on the thermal gradient of the media as well as the magnetic field gradient.[118-121] Also, the high temperatures associated with HAMR can affect other aspects of the device.[122-124] Therefore, a rapid cooling rate is critical to achieve a sharp bit transition. This leads to an important trade-off between fast heating and rapid cooling, which can be tuned with the use of a heat sink layer.

$L1_0$-FePt thin films are a promising candidate for HAMR media due to its high magnetic anisotropy.[125] For a heat sink layer to be incorporated into FePt HAMR media, the material should demonstrate high thermal stability as well as a compatible crystalline structure for $L1_0$-FePt. Both Ag and Cu are well-known as heat sink materials in electronic devices due to their high thermal conductivity of 430 and 400 W/m K, respectively. They also display a low coeffecient of thermal expansion. Also, studies have shown that Ag and Cu have similar crystal structures when sputter deposited.[126] In this work, FePt thin films were grown on both Ag and Cu underlayers to study their

feasibiltiy as heat sink materials. The structure and magnetic properties were investigated, as well as the cross plane thermal conductivity of the FePt thin films.

A. Experiment

The structure of the films was Si/Ag or Cu/Ta (2 nm)/CrRu (25 nm)/MgO (2 nm)/FePt (5nm) prepared by rf (MgO layer) or dc (all other layers) magnetron sputtering. The Ag and Cu heat sink layers were deposited at room temperature with 3 mTorr sputter pressure. The thickness of the heat sink layer was varied at 15, 30, 60, and 120 nm. The Ta layer was deposited at room temperature with a sputter pressure of 10 mTorr, while the CrRu layer was deposited at 300 °C using 3 mTorr sputter pressure. The samples were cooled to room temperature before depositing the MgO layer at 90 °C and the FePt layer at 550 °C, with 5 mTorr and 10 mTorr pressure, respectively. The crystal structure of the films was measured by x-ray diffraction (XRD) while the magnetic properties were measured by a room temperature magneto-optical Kerr effect (MOKE) with an applied field of ± 2.7 Tesla. The thermal diffusivity was measured by a laser-flash technique, where a xenon light source produces a pulse at the surface of the sample, while an InSb infared detector measures the temperature rise on the opposite side. This measures the cross-plane thermal diffusivity through the FePt thin film, which is then calculated into the thermal conductivity using the sample's specific heat and mass density.

B. Results and Discussion

Figures 32 and 33 show the XRD patterns of the FePt thin films grown on Ag [Fig. 32] and Cu [Fig. 33] layers with thicknesses of (a) 15, (b) 30, (c) 60, and (d) 120 nm.

None of the samples grown on the Ag layer exhibited FePt (001) texture, while all samples grown on the Cu layer showed preferred $L1_0$-FePt (001) texture. This is attributed to the fact that the CrRu (002) texture is not formed on the Ag layer, which is necessary to grow FePt (001) perpendicular orientation. Also of note, the samples grown on Ag do not exhibit FePt(111) texture, demonstrating that the FePt films grown on Ag are not perpendicullary oriented nor longitudinally oriented.

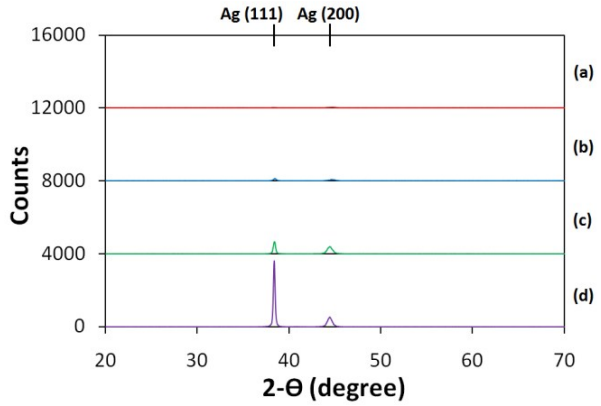

Fig. 32. XRD spectra of FePt thin films grown on a Ag heat sink layer of (a) 15 nm, (b) 30 nm, (c) 60 nm, and (d) 120 nm.

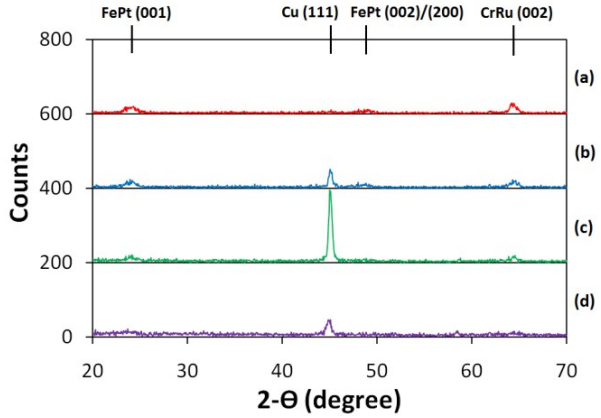

Fig. 33. XRD spectra of FePt thin films grown on a Cu heat sink layer of (a) 15 nm, (b) 30 nm, (c) 60 nm, and (d) 120 nm.

The out-of-plane hysteresis loops of the FePt films grown on Ag and Cu layers with varying thicknesses are shown in Figures 34 and 35, respectively. In both cases, the coercivity of the FePt films decreases as the thickness of the heat sink layer increases. For the FePt films grown on Ag, the coercivity decreases from 1.3 – 1.0 Tesla, while the coercivity decreases from 1.7 – 1.5 Tesla for the FePt films grown on Cu. For the samples grown on Cu, this decrease in coercivity can be attributed to the fact that as the thickness of the Cu layer inreases, both the CrRu (002) and FePt (001) XRD peaks decrease, as seen in Fig. 33. The squareness of the loops of the FePt samples grown on Cu shows perpendicular orientation, while the squareness of the loops grown on Ag shows that the film is rather isotropic, further demonstrated by the fact that both the FePt (001) and FePt (111) peaks are absent in the XRD spectra.

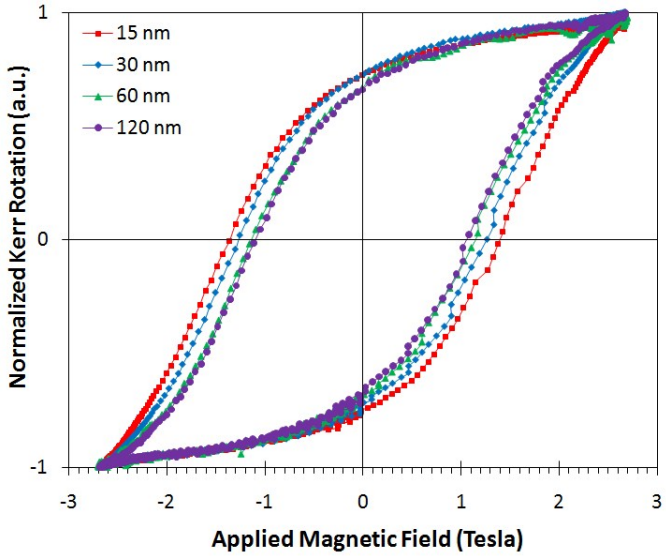

Fig. 34. Out-of-plane hysteresis loops of FePt thin films grown on a Ag heat sink layer of varying thicknesses.

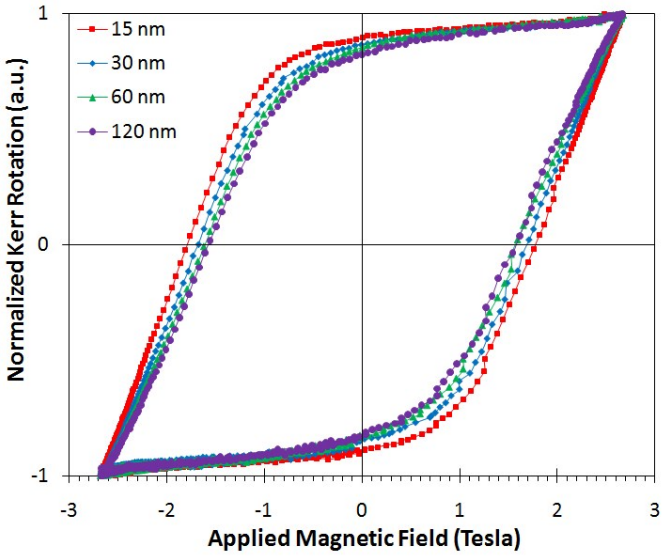

Fig. 35. Out-of-plane hysteresis loops of FePt thin films grown on a Cu heat sink layer of varying thicknesses.

By varying the thickness of the heat sink layer, the thermal properties of the FePt films can be adjusted so that media can be heated quickly to its Curie temperature, but also cooled fast enough to avoid thermal erasure of adjacent tracks. Figure 36 shows the thermal conductivity vs. temperature of the FePt films grown on Ag and Cu layers of 15, 60 and 120 nm thicknesses. A blank Si substrate was also measured for comparison. Since the sample is heated on the surface (FePt layer) but the temperature rise is measured at the opposite side (Si substrate) it is expected that the thermal conductivity for all the samples would decrease compared to the blank Si substrate. This is because the thermal conductivity is measured in the vertical direction of the sample, so that when the FePt films are deposited, some of the heat is dissipated in the horizontal direction, resulting in less heat measured at the bottom end of the sample. As the thickness of the heat sink layer increases, the thermal conductivity decreases, showing that more and more heat is being dissipated horizontally through the heat sink layer. This is especially

true for Cu, where the sample with a 15 nm Cu layer shows much higher thermal conductivity than the other samples. Thus, it can be determined that the thermal properties of the FePt films can be tuned cool faster or slower if desired.

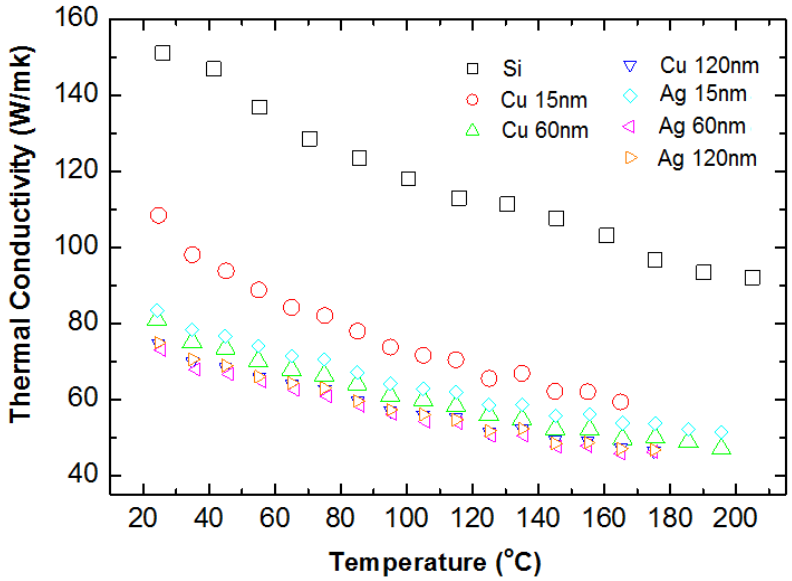

Fig. 36. Cross plane thermal conductivity of FePt thin films grown on Ag and Cu heat sink layers of varying thicknesses.

C. Conclusion

FePt thin films were deposited on Ag or Cu heat sink layers of varying thicknesses for HAMR media. It was found that the $L1_0$-phase was only achieved in the FePt samples grown on Cu while the FePt films grown on Ag appeared to be isotropic. For both the Ag and Cu layers, the coercivity of the FePt films decreased, from 1.3 – 1.0 Tesla and 1.7 – 1.5 Tesla, respectivley, as the thickness increased. Thermal conductivity measurements were made which demonstrated the usefulness of the heat sink layer, as well as the ability to adjust the thermal properties of the FePt layer.

VIII. Multilevel 3-D Magnetic Recording

Traditionally, in order to continually increase the areal density of magnetic recording, scaling laws were implemented. However, eventually scaling will run into the problem known as the superparamagnetic limit, where the size of the grains become so small that they are thermally unstable. Thus, the need for alternative technologies are necessary to keep the magnetic data storage industry relevant. Technologies such as heat-assisted magnetic recording (HAMR)[127,128] and discrete track recording (DTR)[129-131] have been proposed to further increase the areal density. However, with multilevel 3-D (ML3D)[132-134] magnetic recording, areal densities much greater than those promised by HAMR and DTR can be achieved. In ML3D, magnetic layers are stack on top of each other, utilizing not only the surface of the film, but also the volume of the recording media, as seen in Figure 37. This leads to more than two signal levels, as in perpendicular magnetic recording (PMR), allowing for much higher areal densities. The number of signal levels in ML3D depends on the number of magnetic layers in the media, given by the expression

$$M = 2^N, \tag{3}$$

where *N* is the number of magnetic layers. Even with only two magnetic layers, four signal levels are possible, effectively doubling the storage capacity on the same amount of surface area. With three magnetic layers, the storage capacity is quadrupled.

$L1_0$ ordered FePt thin film is a promising candidate for next-generation PMR, as well as HAMR, DTR, and ML3D technologies due to its high magnetic anisotropy.[135] It has been shown that FePt films can achieve coercivities greater than 7 Tesla.[136] This large

range in coercivity is crucial for ML3D, so that each magnetic layer will remain distinct from one another, and that selective switching of individual layers is possible. Also, the magnetic moment of each layer also must be different, so that opposing signals from the top and bottom layers do not cancel each other out. To achieve this, different thicknesses of the layers are used, with the layer underneath it being at least twice as thick as the layer above it. Using FePt in ML3D, more magnetic layers are possible compared to conventional magnetic materials used today, enabling much higher storage capacities. In the present work, a basis for utilizing $L1_0$ FePt in ML3D was formed by fabricating and characterizing dual layer FePt thin films.

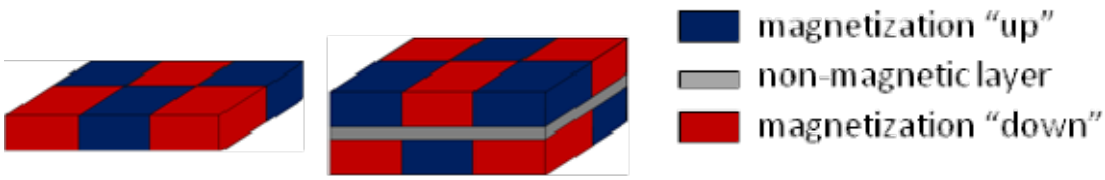

Fig. 37. Comparison of conventional perpendicular media (left) and dual layer multilevel 3-D media (right).

A. Experiment

The bottom FePt layer was fabricated with the structure of Si/CrRu (25 nm)/MgO (6 nm)/FePt (8 nm). The top layer was then deposited on top of the bottom layer with the structure of MgO (4 nm)/FePt (4 nm) or Ta (2 nm)/MgO (4 nm)/FePt (4 nm). The CrRu layer was deposited at 300 °C with 3 mTorr Ar sputter pressure. Both MgO layers in the dual layer films were deposited at 90 °C and 5 mTorr Ar sputter pressure. The Ta layer was deposited at room temperature with 10 mTorr Ar sputter pressure. Both FePt layers were deposited at 550 °C with an Ar sputter pressure of 10 mTorr. Magnetic properties

were measured using a magneto-optical Kerr effect (MOKE) system, while the structural properties were measured by x-ray diffraction (XRD). The surface morphology and magnetic domain structure was characterized by atomic force microscopy (AFM) and magnetic force microscopy (MFM), respectively.

B. Results and Discussion

The the dual layer FePt films were designed so that the coercivity of the bottom layer was much greater than the top layer, for writability purposes, and with the thickness of the bottom layer twice as thick as the top layer, for readback purposes. The next step was to determine a suitable non-magnetic spacing layer between the FePt layers. MgO was chosen as the non-magnetic spacing layer since it has been shown that $L1_0$ FePt can be grown solely on MgO.[137] This ensures that the top layer will be perpendicularly oriented with relatively high coercivity. Figure 38 shows the effects of the MgO spacing layer on the bottom FePt layer. The coercivity of the bottom FePt layer decreases from 1.8 Tesla to 1.5 Tesla with the addition of the MgO spacing layer, and decreases further to 1.4 Tesla when heated to 550 °C, the temperature in which the top FePt will be deposited. When the top FePt layer is deposited at 550 °C, only one hysteresis loop is observed with a coercivity of 0.8 Tesla, as shown in Figure 39. This shows that the two magnetic layers are magnetically coupled and act as a single magnetic layer. However, when the top FePt layer is deposited at room temperature, a dual-phase hysteresis loop is observed, albeit with the top layer magnetically soft. Thus, the thickness of the MgO spacing layer was sufficient to separate the two magnetic layers so they are magnetically decoupled, but become coupled together due to the high sputter temperature of the top

FePt layer. It was concluded that as the sample is heated to 550 °C, the MgO layer begins to mix into the FePt layers effectively decreasing the spacing between the two magnetic layers allowing them to become magnetically coupled. This mixing of MgO in FePt is similar to the work purposefully done to develop FePt-MgO granular media.[138-143]

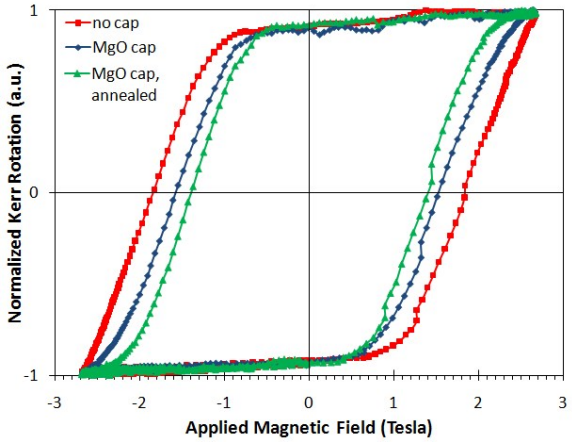

Fig. 38. Out-of-plane hysteresis loops of the bottom FePt layer only, the bottom FePt layer with MgO spacing layer, and the bottom FePt layer with MgO spacing layer annealed at 550 °C.

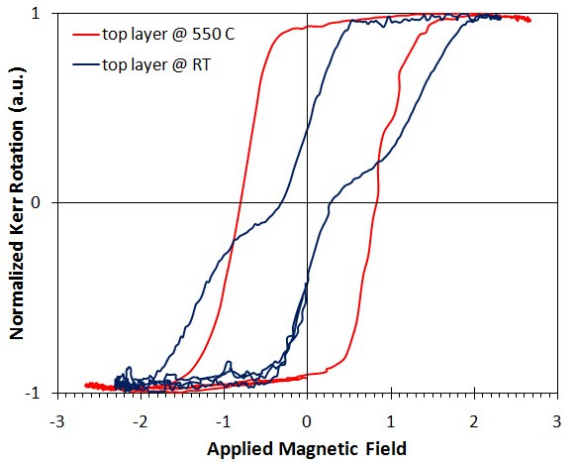

Fig. 39. Out-of-plane hysteresis of the dual layer FePt thin film with the structure of Si/CrRu/MgO/FePt/MgO/FePt, with the top FePt layer deposited at 550 °C and room temperature.

In order to prevent this intermixing of MgO and FePt, a Ta layer was introduced. Figure 40 shows the effects of the Ta layer when deposited on top of the bottom FePt

layer. The coercivity of the FePt layer increases slightly from 1.9 Tesla to 2.0 Tesla with the addition of the Ta layer, and remains almost unchanged when heated to 550 °C. Using MgO as a seed layer, the top FePt layer was deposited on top of the Si/CrRu/MgO/FePt/Ta film as shown in Figure 41. The resulting film showed dual-phase hysteresis, as shown in Figure 42. Minor loops were also measured which showed the top layer of having a coercivity of 0.5 Tesla. The bottom layer showed a coercivity of 1.35 Tesla.

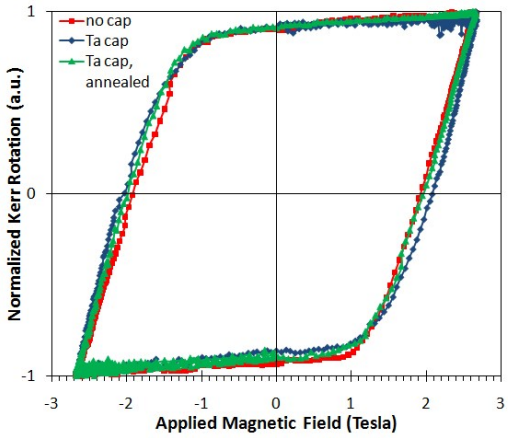

Fig. 40. Out-of-plane hysteresis loops of the bottom FePt layer only, the bottom FePt layer with Ta layer, and the bottom FePt layer with Ta layer annealed at 550 °C.

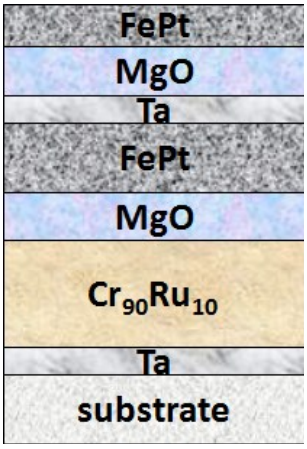

Fig. 41. Simple schematic of the dual layer FePt film using a Ta/MgO non-magnetic spacing layer.

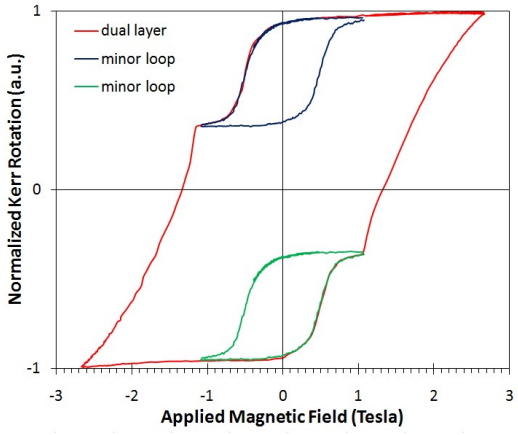

Fig. 42. Out-of-plane hysteresis loop of the dual layer FePt thin film with the structure of Si/CrRu/MgO/FePt/Ta/MgO/FePt along with minor loops of the top FePt layer.

Figure 43 shows the XRD spectra of the dual layer FePt film with a Ta/MgO spacing layer. A strong FePt (001) peak is observed while a FePt (111) peak is not, suggesting that both layers are in the $L1_0$-phase. Figure 44 shows a 1.5 × 1.5 μm^2 AFM and MFM image of the dual layer film. The surface roughness of the film was 1.96 nm. Figure 45 shows the section analysis (white line in Figure 44) of the dual layer FePt film. From the section analysis, four signal levels are observed, which come from the different possible combinations of the magnetization of the two magnetic layers. The two signals were the magnetic layers are oppositely oriented do not cancel out due to the difference in thickness, which leads to different magnetic moments.

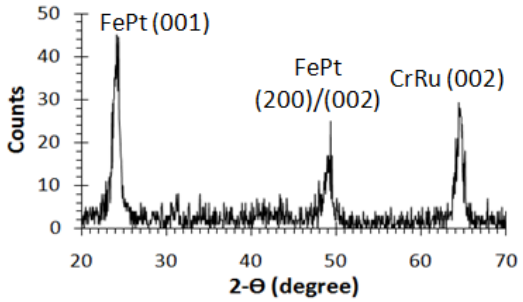

Fig. 43. XRD spectra of the Si/CrRu/MgO/FePt/Ta/MgO/FePt dual layer film.

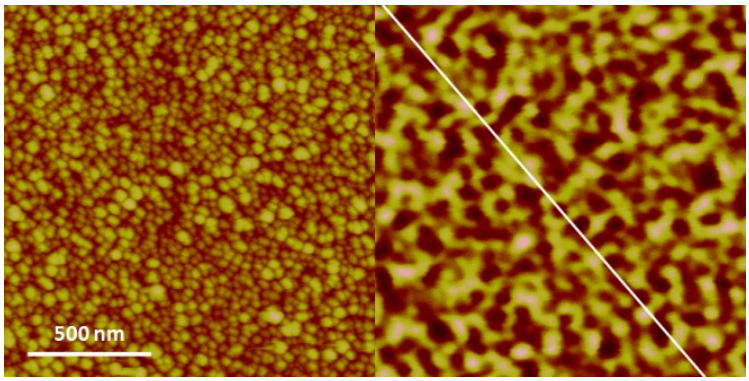

Fig. 44. 1.5 × 1.5 μm^2 AFM (left) and MFM (right) image of the dual layer film with structure of Si/CrRu/MgO/FePt/Ta/MgO/FePt.

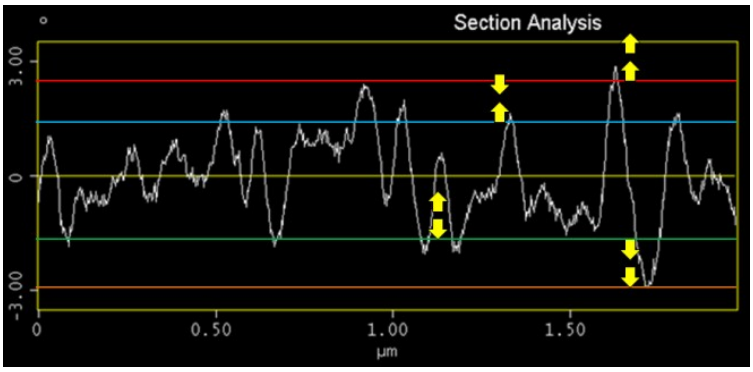

Fig. 45. Section analysis of the 1.5 × 1.5 μm^2 MFM image demonstrating the four signal levels of the dual layer FePt film.

C. Conclusion

Dual layer FePt films were fabricated and characterized for the use in multilevel 3-D magnetic recording. MgO was used as the non-magnetic spacing layer because of its ability to induce the $L1_0$-phase of the top FePt layer. However, as the sample was heated to 550 °C, the MgO mixed with the FePt layers causing magnetic coupling between the two layers. This issue was solved by first depositing a thin Ta layer on top of the bottom FePt layer, then depositing the MgO and FePt layers. The dual layer structure showed a dual-phase hysteresis loop with the bottom layer having a coercivity of 1.35 Tesla and the

top layer exhibiting 0.5 Tesla coercivity. MFM showed four distinct signal levels with domain sizes as small as 50 nm in diameter, thus, demonstrating the capability of dual layer FePt media for 3-D magnetic recording.

IX. Overview

An introduction to magnetism and the hard disk drive industry was given as a means for understanding the work in this dissertation. $L1_0$-FePt thin films were fabricated and characterized as a next-generation perpendicular magnetic recording material. The surface roughness of the FePt films was improved, and the sputtering conditions of the FePt layer and its underlayers were optimized to obtain high coercivity media and as thin a film as possible. A substrate-patterning process was developed in order to utilize FePt thin films as bit-patterned media. Also, FePt thin films were fabricated using a heat sink layer for heat-assisted magnetic recording. Lastly, a dual layer FePt structure was fabricated for its use in 3-D magnetic recording. While much work remains to be done, this dissertation showed that FePt can be used as a next-generation magnetic recording material, as well as for future technologies currently being investigated by the hard disk drive industry.

References

[1]S.N. Piramanayagam, J. Appl. Phys. **102** 011301 (2007).

[2]S. Iwasaki and K. Takemura, IEEE Trans. Magn. **11**, 1173 (1975).

[3]S. Iwasaki and Y. Nakamura, IEEE Trans. Magn. **14**, 436 (1978).

[4]S. Iwasaki, Y. Nakamura, and K. Ouchi, IEE Trans. Magn. **15**, 1456 (1979).

[5]D. E. Laughlin, Y. C. Feng, D. N. Lambeth, L. L. Lee, and L. Tang, J. Magn. Magn. Mater. **155**, 146 (1996).

[6]L. L. Lee, D. E. Laughlin, L. Fang, and D. N. Lambeth, IEEE Trans. Magn. **31**, 2728 (1995).

[7]B. R. Acharya, A. Inomata, E. N. Abarra, A. Ajan, D. Hasegawa, and I. Okamoto, J. Magn. Magn. Mater. **260**, 261 (2003).

[8]B. R. Acharya, E. N. Abarra, and I. Okamoto, IEEE Trans. Magn. **37**, 1475 (2001).

[9]M. Zheng, B. R. Acharya, G. Choe, J. N. Zhou, Z. D. Yang, E. N. Abarra, and K. E. Johnson, IEEE Trans. Magn. **40**, 2498 (2004).

[10]G. Choe, IEEE Trans. Magn. **31**, 2809 (1995).

[11]B. B. Lal, M. Tobise, and T. Shinohara, IEEE Trans. Magn. **30**, 3954 (1994).

[12]T. Kanbe, Y. Takahashi, K. Tanahashi, A. Ishikawa, and Y. Hosoe, IEEE Trans. Magn. **35**, 2667 (1999).

[13]T. Kanbe, Y. Yahisa, H. Suzuki, H. Kataoka, Y. Takahashi, and Y. Hirayama, J. Appl. Phys. **91**, 8611 (2002).

[14]S. N. Piramanayagam, Y. F. Xu, D. Y. Dai, L. Huang, S. I. Pang, and J. P. Wang, J. Appl. Phys. **91**, 7685 (2002).

[15]D. Djayaprawira, M. Mikami, S. Yoshimura, and A. Takahashi, IEEE Trans. Magn. **39**, 2258 (2003).

[16]L. L. Lee, D. E. Laughlin, and D. N. Lambeth, IEEE Trans. Magn. **34**, 1561 (1998).

[17]Y. F. Xu, J.P. Wang, C. K. Pock, X. M. Cheng, Z. S. Shan, and T. C. Chong, IEEE Trans. Magn. **37**, 1491 (2001).

[18]D. Weller and M. F. Doerner, Annu. Rev. Mater. Sci. **30**, 611 (2000).

[19]T. Kanbe, I. Tamai, Y. Takahashi, K. Tanahashi, Y. Hosoe, A. Ishikawa, and H. Kataoka, IEEE Trans. Magn. **33**, 2980 (1997).

[20]E. W. Singleton and P. B. Narayan, J. Appl. Phys. **85**, 5840 (1999).

[21]S. Ohkijima, M. Oka, and H. Murayama, IEEE Trans. Magn. **33**, 2944 (1997).

[22]T. Yogi and T. A. Nguyen, IEEE Trans. Magn. **29**, 307 (1993).

[23]N. Inaba and M. Futamoto, J. Appl. Phys. **87**, 6863 (2000).

[24]C. R. Paik, I. Suzuki, N. Tani, M. Ishikawa, Y. Ota, and K. Nakamura, IEEE Trans. Magn. **28**, 3084 (1992).

[25]M. P. Sharrock, J. Appl. Phys. **76**, 6413 (1994).

[26]G. Bayreuther, P. Bruno, G. Lugert, D. Renard, and C. Turtur, Thin Solid Films **175**, 341 (1989).

[27]B. R. Acharya, J. N. Zhou, M. Zheng, G. Choe, E. N. Abarra, and K. E. Johnson, IEEE Trans. Magn. **40**, 2383 (2004).

[28]M. Zheng, G. Choe, A. Chekanov, B. G. Demczyk, B. R. Acharya, and K. E. Johnson, IEEE Trans. Magn. **39**, 1919 (2003).

[29]T. Oikawa, M. Nakamura, H. Uwazumi, T. Shimatsu, H. Muraoka, and Y. Nakamura, IEEE Trans. Magn. **38**, 1976 (2002).

[30]H. Yamane, S. Watanabe, J. Ariake, N. Honda, K. Ouchi, and S. Iwasaki, J. Magn. Magn. Mater. **287**, 153 (2004).

[31]T. Shimatsu, H. Sato, T. Oikawa, K. Mitsuzuka, Y. Inaba, O. Kitakami, S. Okamoto, H. Aoi, H. Muraoka, and Y. Nakamura, IEEE Trans. Magn. **41**, 3175 (2005).

[32]Y. Inaba, T. Shimatsu, T. Oikawa, H. Sato, H. Aoi, H. Muraoka, and Y. Nakamura, IEEE Trans. Magn. **40**, 2486 (2004).

[33]I. Takekuma, R. Araki, M. Igarashi, H. Nemoto, I. Tamai, Y. Hirayama, and Y. Hosoe, J. Appl. Phys. **99**, 08E713 (2006).

[34]J. R. Desserre, IEEE Trans. Magn. **20**, 663 (1984).

[35]N. Amos, R. Fernandez, R. Ikkawi, B. Lee, A. Lavrenov, A. Krichevsky, D. Litvinov, and S. Khizroev, J. Appl. Phys. **103**, 07E732 (2008).

[36]Y. Hirayama, M. Futamoto, K. Kimoto, and K. Usami, IEEE Trans. Magn. **32**, 3807 (1996).

[37]Y. Hirayama, Y. Honda, T. Takeuchi, and M. Futamoto, IEEE Trans. Magn. **35**, 2766 (1999).

[38]H. Uwazumi, T. Shimatsu, Y. Sakai, A. Otsuki, I. Watanabe, H. Muraoka, and Y. Nakamura, IEEE Trans. Magn. **37**, 1595 (2001).

[39]J. Ariake, N. Honda, K. Ouchi, and S. I. Iwasaki, IEEE Trans. Magn. **36**, 2411 (2000).

[40]G. A. Bertero D. Wachenschwanz, S. Malhotra, S. Velu, B. Bian, D. Stafford, Y. Wu, T. Yamashita, and S. X. Wang, IEEE Trans. Magn. **38** 1627 (2002).

[41]N. Honda, J. Ariake, K. Ouchi, and S. Iwasaki, IEEE Trans. Magn. **30**, 4023 (1994).

[42]N. Honda, J. Ariake, and K. Ouchi, IEEE Trans. Magn. **34**, 1651 (1998).

[43]Y. Hirayama, M. Futamoto, K. Ito, Y. Honda, and Y. Maruyama, IEEE Trans. Magn. **33**, 996 (1997).

[44]T. Shimatsu, H. Sato, T. Oikawa, K. Mitsuzuka, Y. Inaba, O. Kitakami, S. Okamoto, H. Aoi, and H. Muraoka, IEEE Trans. Magn. **41**, 3175 (2005).

[45]Y. Inaba, T. Shimatsu, S. Oikawa, H. Sato, H. Aoi, H. Muraoka, and Y. Nakamura, IEEE Trans. Magn. **40**, 2486 (2004).

[46]H. Uwazumi, N. Nakajima, M. Masuda, T. Kawata, S. Takenoiri, S. Watanable, Y. Sakai, and K. Enomoto, IEEE Trans. Magn. **40**, 2392 (2004).

[47]T. Shimatsu, H. Sato, T. Oikawa, Y. Inaba, O. Kitakami, S. Okamoto, H. Aoi, and H. Muraoka, and Y. Nakamura, IEEE Trans. Magn. **41** 566 (2005).

[48]T. Shimatsu, T. Oikawa, Y. Inaba, H. Sato, I. Watanabe, H. Aoi, H. Muraoka, and Y. Nakamura, IEEE Trans. Magn. **40**, 2461 (2004).

[49]Y. Inaba, T. Shimatsu, H. Muraoka, J. D. Dutson, and K. O'Grady, IEEE Trans. Magn. **41**, 3130 (2005).

[50]B. X. Xu, H. X. Yuan, J. Zhang, J. P. Yang, R. Ji, and T. C. Chong, J. Appl. Phys. **103**, 07F525 (2008).

[51]O. A. Ivanov, L. V. Solina, V. A. Demshina, and L. M. Magat, Fiz. Met. Metalloved, **35**, 81 (1973).

[52]D. Weller, A. Moser, L. Folks, M. E. Best, W. Lee, M. F. Toney, M. Schwickert, J. U. Thiele, M. F. Doerner, IEEE Trans. Magn. **36**, 10 (2000).

[53] Y. Xu, J. S. Chen, and J. P. Wang, Appl. Phys. Lett. **80**, 3325 (2002).

[54] M.-G. Kim, S.-C. Shin, and K. Kang, Appl. Phys. Lett. **80**, 3802 (2002).

[55] J. S. Chen, B. C. Lim, and J. P. Wang, Appl. Phys. Lett. **81**, 1848 (2002).

[56] B. C. Lim, J. S. Chen, and J. P. Wang, Surf. & Coat. Technol. **198**, 296 (2005).

[57] W. K. Shen, J. H. Judy, and J.-P. Wang, J. Appl. Phys. **97**, 10H301 (2005).

[58] B. C. Lim, J. S. Chen, and G. M. Chow, IEEE Trans. Magn. **42**, 3017 (2006).

[59] Z. Lu, M. J. Walock, P. LeClair, W. H. Butler, and G. J. Mankey, J. Vac. Sci. Technol., **27**, 1067 (2009).

[60] H. Wang, F. J. Yang, Q. Mo, J. Zhang, H. B. Wang, Y. Wang, J. Magn. Magn. Mater. **321**, 2627 (2009).

[61] J. S. Chen, Y. Xu, and J. P. Wang, J. Appl. Phys. **93**, 1661 (2003).

[62] Z. L. Zhao, J. S. Chen, J. Ding, J. B. Yi, B. H. Liu, J. P. Wang, Appl. Phys. Lett. **88**, 052503 (2006).

[63] J. S. Chen, B. C. Lim, J. F. Hu, Y. K. Lim, B. Liu, G. M. Chow, Appl. Phys. Lett. **92**, 042508 (2007).

[64] B. C. Lim, J. S. Chen, J. F. Hu, Y. K. Lim, B. Liu, G. M. Chow, G. Ju, J. Appl. Phys. **103**, 07E143 (2008).

[65] S.-W. Wang, A. C. Sun, F.-T. Yuan, J.-H. Hsu, and P.-C. Kuo, IEEE Trans. Magn. **45**, 3580 (2009).

[66] X. H. Li, B. T. Liu, H. Y. Sun, W. Li, and X. Y. Zhang, J. Phys. D: Appl. Phys. **41**, 135009 (2008).

[67] E. Yang, and D. E. Laughlin, J. Appl. Phys. **104**, 023904 (2008).

[68] Y. F. Ding, J. S. Chen, B. C. Lim, J. F. Hu, B. Liu, G. Ju, Appl. Phys. Lett. **93**, 032506 (2008).

[69]J. S. Chen, J. F. Hu, B. C. Lim, Y. F. Ding, G. M. Chow, G. Ju, IEEE Trans. Magn. **45**, 839 (2009).

[70] J. S. Chen, B. C. Lim, Y. F. Ding, J. F. Hu, G. M. Chow, G. Ju, J. Appl. Phys. **105**, 07B702 (2009).

[71] A. Perumal, Y. K. Takahashi, and K. Hono, J. Appl. Phys. **105**, 07B732 (2009).

[72] X. Li, G. Wang, Y. Liu, L. Xu, J. Zhao, B. Liu, X. Zhang, Appl. Phys. Lett. **94**, 172512 (2009).

[73]S. H. Lee, J. K. Park, Mater. Chem. and Phys. **118**, 213 (2009).

[74]S. N. Piramanayagam and K. Srinivasan, Appl. Phys. Lett. **91**, 142508 (2007).

[75] S. Khizroev and D. Litvinov, J. Appl. Phys. **95**, 4521 (2004).

[76] R. Wood, IEEE Trans. Magn. **36**, 36 (2000).

[77]A. Kikitsu, Y. Kamata, M. Sakurai, and K. Naito, IEEE Trans. Magn. **43**, (2007) 3685.

[78]M. Kryder, E. Gage, T. McDaniel, W. Challener, R. Rottmayer, G. Ju, Y.-T. Hsia, and M. F. Erden, Proceed. IEEE **96**, (2008) 1810.

[79]N. Amos, R. Ikkawi, A. Krichevsky, R. Fernandez, E. Stefanescu, I. Dumer, D. Litvinov, and S. Khizroev, J. Nanoelect. Optoelect. **2**, (2007) 257.

[80]D. Weller, A. Moser, L. Folks, M. E. Best, W. Lee, M. F. Toney, M. Schwickert, J.-U. Thiele, and M. F. Doerner, IEEE Trans. Magn. **36**, (2000) 10.

[81]T. Shima, K. Takanashi, Y. K. Takahashi, and K. Hono, Appl. Phys. Lett. **85**, (2004) 2571.

[82]Y. N. Hsu, S. Jeong, D. E. Laughlin, and D. N. Lambeth, J. Appl. Phys. **89**, (2001) 7068.

[83]H. Y Sun, J. L. Xu, S. Z. Feng, Z. F. Su, J. Hu, and Y. P. Sun, Appl. Phys. Lett. **88**, (2006) 192501.

[84]Feng, B. H. Li, G. Han, J. Teng, Y. Jiang, Q. L. Liu, and G. H. Yu, Appl. Phys. Lett. **88**, (2006) 232109.

[85]Y. F. Xu, J. S. Chen, and J. P. Wang, Appl. Phys. Lett. **80**, (2002) 3325.

[86]H. Lai, C. C. Chiang, T. Balaji, and T. K. Tseng, Appl. Phys. Lett. **85**, (2004) 4430.

[87]Y. Zhu and J. W. Cai, Appl. Phys. Lett. **87**, (2005) 032504.

[88]Y. C. Lai, Y. H. Chang, Y. C. Chen, C. H. Liang, W. C. Chang, C. M. Chiou, and G. J. Chen, J. Appl. Phys. **101**, (2007) 053913.

[89]C. Chiang, C. H. Lai, and Y. C. Wu, Appl. Phys. Lett. **88**, (2006) 152508.

[90]S. Jeong, Y. N. Hsu, M. E. McHenry, and D. E. Laughlin, J. Appl. Phys. **87**, (2000) 6950.

[91]J. S. Chen, B. C. Lim, and J. P. Wang, Appl. Phys. Lett. **81**, (2002) 1848.

[92]Z. G. Zhang, K. Kang, and T. Suzuki, Appl. Phys. Lett. **83**, (2003) 1785.

[93]H. Wei, F. T. Yuan, H. W. Chang, and Y. D. Yao, J. Appl. Phys. **103**, (2008) 07E138.

[94]B. C. Lim, J. S. Chen, and J. P. Wang, Surface & Coatings Technology **198**, (2005) 296.

[95]B. C. Lim, J. S. Chen, and G. M. Chow, IEEE Trans. Magn. **42**, (2006) 3017.

[96]B. C. Lim, J. S. Chen, J. F. Hu, Y. K. Lim, B. Liu, G. M. Chow, and G. Ju, J. Appl. Phys. **103**, (2008) 07E143.

[97]Y. F. Ding, J. S. Chen, B. C. Lim, J. F. Hu, B. Liu, and G. Ju, Appl. Phys. Lett. **93**, (2008) 032506.

[98]J. S. Chen, B. C. Lim, Y. F. Ding, J. F. Hu, G. M. Chow, and G. Ju, J. Appl. Phys. **105**, (2009) 07B702.

[99]D. Litvinov, J. Wolfson, J. A. Bain, R. W. Gustafson, M. H. Kryder, and S. Khizroev, IEEE Trans. Magn. **38**, (2002) 1658.

[100]D. Litvinov, A. Lyberatos, J. Wolfson, J. A. Bain, and S. Khizroev, IEEE Trans. Magn. **38**, (2002) 1994.

[101]D. Litvinov, J. Wolfson, J. A. Bain., R. W. Gustafson, M. H. Kryder, and S. Khizroev, **38**, (2002) 2253.

[102]S. Khizroev and D. Litvinov, J. Appl. Phys. **95**, (2004) 4521.

[103]S. Khizroev, Y. Hijazi, N. Amos, E. Felissaint, N. Joshi, R. Ikkawi, R. Chomko, and D. Litvinov, J. Nanosci. Nanotechnol. **7**, (2007) 1.

[104]M. T. Moneck, J.-G. Zhu, X. Che, Y. Tang, H. J. Lee, S. Zhang, K.-S. Moon, and N. Takahashi, IEEE Trans. Magn. **43**, 2127 (2007).

[105]A. Kikitsu, Y. Kamata, M. Sakurai, and K. Naito, IEEE Trans. Magn. **43**, 3685 (2007).

[106]R. Sbiaa, E. L. Tan, R. M. Seoh, K. O. Aung, S. K. Wong, and S. N. Piramanayagam, J. Vac. Sci. Technol. B. **26(5)**, 1666 (2008).

[107]K. Moon, X. Che, Y. Tang, H. Lee, Y. Tang, M. T. Moneck, J.-G. Zhu, and N. Takahashi, IEEE Trans. Magn. **44**, 3442 (2008).

[108]Y. Tang, X. Che, H. J. Lee, and J.-G. Zhu, IEEE Trans. Magn. **44**, 4780 (2008).

[109]M. Hashimoto, K. Miura, H. Muraoka, H. Aoi, R. Wood, M. Salo, and Y. Ikeda, J. Magn. Magn. Mater. **320**, 2935 (2008).

[110]S.-J. Yoon, S.-H. Son, J. Kang, H. Kim, J. Yoo, and D.-H. Choi, IEEE Trans. Magn. **45**, 2296 (2009).

[111]Y. Kanai and K. Yamakawa, J. Magn. Magn. Mater. **321**, 518 (2009).

[112]S. Takenoiri, J. Magn. Magn. Mater. **321**, 562 (2009).

[113]S. Greaves, Y. Kanai, and H. Muraoka, IEEE Trans. Magn. **46**, 1460 (2010).

[114]B. A. Gurovich, K. E. Prikhodko, E. A. Kuleshova, A. Y. Yakubovsky, E. Z. Meilikhov, and M. G. Mosthenko, J. Magn. Magn. Mater. **322**, 3060 (2010).

[115]A. Ajan, K. Sato, N. Aoyama, T. Tanaka, Y. Miyaguchi, K. Tsumagari, T. Morita, T. Nishihashi, A. Tanaka, and T. Uzumaki, IEEE Trans. Magn. **46**, 2020 (2010).

[116]M. A. Seigler, W. A. Challener, E. Gage, N. Gokemeijer, G. Ju, B. Lu, K. Pelhos, C. Peng, R. E. Rottmayer, X. Yang, H. Zhou, and T. Rausch, IEEE Trans. Magn. **44**, 119 (2008).

[117]M. H. Kryder, E. C. Gage, T. W. McDaniel, W. A. Challener, R. E. Rottmayer, G. Ju, Y.-T. Hsia, and M. F. Erden, Proceed. IEEE **96**, 1810 (2008).

[188]T. W. McDaniel, W. A. Challener, and K. Sendur, IEEE Trans. Magn. **39**, 1972 (2003).

[119]A. Lyberatos and J. Hohlfeld, J. Appl. Phys. **95**, 1949 (2004).

[120]F. Akagi, T. Matsumoto, and K. Nakamura, J. Appl. Phys. **101**, 09H501 (2007).
[121]B. Xu, H. Yuan, J. Zhang, R. Ji, Q. Zhang, X. Miao, and T. C. Chong, J. Magn. Magn. Mater. **320**, 731 (2008).

[122]L. Wu, Nanotechnology **18**, 215702 (2007).

[123]S. J. Greaves and H. Muraoka, J. Appl. Phys. **101**, 09H502 (2007).

[124]B. X. Xu, H. X. Yuan, J. Zhang, J. P. Yang, R. Ji, and T. C. Chong, J. Appl. Phys. **103**, 07F525 (2008).

[125]D. Weller, A. Moser, L. Folks, M. E. Best, W. Lee, M. F. Toney, M. Schwickert, J.-U. Thiele, and M. F. Doerner, IEEE Trans. Magn. **36**, 10 (2000).

[126]A. Zendehnam, M. Ghanati, and M. Mirzaei, J. Phys.: Conf. Series **61**, 1322 (2007).

[127]M. A. Seigler, W. A. Challener, E. Gage, N. Gokemeijer, G. Ju, B. Lu, K. Pelhos, C. Peng, R. E. Rottmayer, X. Yang, H. Zhou, and T. Rausch, IEEE Trans. Magn. **44**, 119 (2008).

[128]M. H. Kryder, E. C. Gage, T. W. McDaniel, W. A. Challener, R. E. Rottmayer, G. Ju, Y.-T. Hsia, and M. F. Erden, Proceed. IEEE **96**, 1810 (2008).

[129]A. Kikitsu, Y. Kamata, M. Sakurai, and K. Naito, IEEE Trans. Magn. **43**, 3685 (2007).

[130]M. T. Moneck, J.-G. Zhu, X. Che, Y. Tang, H. J. Lee, S. Zhang, K.-S. Moon, and N. Takahashi, IEEE Trans. Magn. **43**, 2127 (2007).

[131]K. Moon, X. Che, Y. Tang, H. Lee, Y. Tang, M. T. Moneck, J.-G. Zhu, and N. Takahashi, IEEE Trans. Magn. **44**, 3442 (2008).

[132]V. Baltz, S. Landis, B. Rodmacq, and B. Dieny, J. Magn. Magn. Mater. **290**, 1286 (2005).

[133]S. Khizroev, Y. Hijazi, N. Amos, and R. Chomko J. Appl. Phys. **100**, 063907 (2006).

[134]S. Khizroev, Y. Hijazi, N. Amos, D. Doria, A. Lavrenov, R. Chomko, T. M. Lu, and D. Litvinov, J. Nanoelect. Optoelect. **1**, 1 (2008).

[135]J. S. Chen, B. C. Lim, J. F. Hu, Y. K. Lim, B. Liu, and G. M. Chow, Appl. Phys. Lett. **90**, 042508 (2007).

[136]T. Shima, K. Takanashi, Y. K. Takahashi, and K. Hono, Appl. Phys. Lett. **85**, 2571 (2005).

[137]Z. L. Zhao, J. S. Chen, J. Ding, J. B. Yi, B. H. Liu, and J. P. Wang, Appl. Phys. Lett. **88**, 052503 (2006).

[138]T. Suzuki, Z. Zhang, A. K. Singh, J. Yin, A. Perumal, and H. Osawa, IEEE Trans. Magn. **41**, 555 (2005).

[139]D.H. Wei, K.L. You, Y.D. Yao, D.P. Chiang, Y. Liou, T.S. Chin, and C.C. Yu, J. Magn. Magn. Mater. **310**, e753 (2007).

[140]A.-C. Sun, J.-H. Hsu, P.C. Kuo, and H.L. Huang, IEEE Trans. Magn. **43**, 2130 (2007).

[141]T. Shima, K. Takanashi, Y.K. Takahashi, and K. Hono, Appl. Phys. Lett. **88**, 063117 (2006).

[142]A.-C. Sun, Y.C. Tsai, F.-T. Yuan, J.-H. Hsu, and P.C. Kuo, IEEE Trans. Magn. **44**, 3531 (2008).

[143]H. J. Kim, K. Kim, S.-R. Lee, and W. Y. Jeung, IEEE Trans. Magn. **44**, 3535 (2008).